Mass Selective Capture by an RFQ Trap of Externally Injected Ions

by

Louise Davey

A thesis submitted to the faculty of Graduate Studies and Research
in partial fulfillment of the requirements for the degree of Master of Science.

Foster Radiation Laboratory
Department of Physics
McGill University, Montreal

March 1992

ABSTRACT

A system for mass-selective capture of ions by a Paul trap was designed and tested.

An Paul trap and associated electronics have been assembled and tested, selectively trapping the ionic clusters C^+_2 and C^+_3 from a pulsed laser ion source. The ions were injected at 90 eV, trapped, extracted and detected, several parameters related to these processes were investigated. Simple models of the injection mechanism employed and for evaluating the pseudo-potential well depth of the ion trap are proposed. The overall efficiency of the ion injection system has been evaluated and compared to other methods of ion capture by an RFQ trap from an external source.

RESUME

Une système pour sélectivement capturée les ions dans une piège à ions de type Paul a été construit et testée.

Une piège à ions de type Paul et éléctroniques associées ont été montés et testés, piègant sélectivement les clusters ioniques C_{2+} et C_{3+} à partir d'une source d'ions à laser pulsé. Les ions ont été injectés à 90 eV, piégés, extraits et detectés. Plusieurs parametres relatif à ces processus ont été examinés. Des models simples ont été proposés pour étudier le mechanisme d'injection et pour évaluer la puit pseudopotentiel du piège a ions. L'éfficacité totale du systeme d'injection d'ions à été évaluée et comparée à d'autres méthodes de capturé des ions avec une piège de type Paul à partire d'une source externe.

ACKNOWLEDGEMENTS

I would like to thank my supervisors Professors J.K.P. Lee and John Crawford for their guidance. Special thanks is due to Professor Lee for his patience and great generosity with his time over the course of this project.

I would like to acknowledge Leo Nikkinen and Steve Kikani for their invaluable technical assistance and teachings. I greatly appreciate Stella Laleff's help with the typing.

Hearty thanks go to Dave Lunney for sharing his knowledge with me over many lengthy discussions, a few about physics.

Finally I would like to thank Pascal for his encouragement and his patience throughout this period and my mom for her unfaltering support of this (and even a few less noble) endeavor.

TABLE OF CONTENTS

TABLE OF FIGURES

LIST OF TABLES

Chapter I

Introduction

There is a great interest in confining particles for study. It is a particularly advantageous prospect for work with rare and exotic matter which is only available in limited quantities. One way to confine charged particles is with electromagnetic (EM) traps. There are two widely used varieties of electromagnetic traps: the Penning trap which utilises both electric and magnetic fields to confine charged particles, and the Paul trap which employs electric fields exclusively. By using an EM trap, long term interactions of charged particles with external fields can be studied.

The Paul trap, also known as the Radio Frequency Quadrupole (RFQ) trap can be more practical in some instances than the Penning trap which requires the maintenance of strong and highly uniform magnetic fields. First patented by Paul and Steinweder in 1956 (PA56) the RFQ trap has since been fully integrated into the realm of Mass and Laser Spectroscopy where it is employed extensively both as a containment device as well as for direct measurements of fundamental particle properties such as mass. It has been demonstrated suitable for ultra-precise experimental work, providing a well defined and stable environment. Notably it was employed to measure the hyperfine splitting of energy levels (MC78).

The RFQ trap consists of three electrodes: a ring enclosed by, but isolated from, two endcaps.

Ions are confined by an electric field created by a radio-frequency (RF) potential to the ring relative to the two endcaps. There are many facets of interest to explore in the workings of the RFQ trap, one of interest is how to introduce ions into the electric field of the trap. The most common methods to place ions inside the trap created them inside the trap. The standard techniques used were Electron Impact (EI) and Chemical Ionization (CI) and more recently the Laser Desorption (LD) technique has been applied [(GI91), (GL89), (HE89), (KW89), (LO89)]. Ions are produced using the EI technique when a gas, diffused inside the trap, is bombarded with an electron beam. This is a highly effective though non-discriminating method of ion production. In the CI process they are created from reactive gases mixed within the confines of the trap. Though this method offers highly selective ion creation its application is limited since not all particles intended for study are the products of reagents. Using the LD technique ions are produced by irradiating a sample surface with a high powered laser. This method has an advantage in that a large variety of samples can be vaporised. However like the EI technique the ion production is non-selective and the source can include a large variety of particles.

There are many cases where sample purity is important to the experiment. In high resolution spectroscopic studies, for example, it may be absolutely essential to confine only one element, or even a single isotope. Non-discriminating internal production methods must rely on a mass selective ejection process, as was demonstrated by Louris et al. (LO90), to weed out undesired ions from the trap. Though this method has been shown effective there are clearly advantages to creating the ions externally and injecting only a targeted mass group into the trap.

There are several difficulties associated with capturing ions from an externally created source. The problem has received considerable theoretical attention [(CH80), (CH82), (CS80), (LU89), (MO89), (TO80)] though only recently has it actually been attempted experimentally. The various models developed used numerical methods to investigate three cases of ion injection: through the gap between ring and endcap electrodes, through an aperture in the ring electrode, and through an aperture in one of the endcap electrodes. The stability of the injected ion was determined by mapping its trajectory inside the field region. If an injected ion was able to remain in the cavity of the trap for more than a given number of RF cycles, 20 000 cycles in

the case of Todd et al. (TO80), it was considered stable.

The results as to the feasibility of each injection method are conflicting and comparisons among the different calculated results are difficult since the trapping procedures and conditions varied greatly from study to study. It is however an agreement of all theoretical analyses that the capture of externally injected ions by the RFQ trap for is strongly dependent on their energy and the timing of injection. The discrimination due to the timing of injection is due to the periodic nature of the confining field. Furthermore, it was calculated by (CS81) that no injected ion can remain trapped indefinitely unless its kinetic energy is reduced once inside the trap. That is to say, the trajectories of injected ions satisfying the initial energy and timing conditions eventually surpass the limits of the confining fields unless they are retarded once inside the trap.

The calculated phase angle for successful injection is typically only on the order of few degrees of the cycle [(LU89), (CH83), (CS81)]. The implications of this is that ion capture could only be efficient for pulsed ion injection.

Despite these findings almost all the work to date on the injection of ions into an RFQ trap has employed DC ion beams. In DC injection a continuous beam of ions is directed through the centre of the trap, individual ions that are able to reduce their kinetic energy inside the cavity have a probability of being trapped. Usually the cavity is filled with a light buffer gas such as helium or neon and some injected ions are expected to reduce their energy through collisions with these particles. The cyclical nature of ion capture by the RFQ trap means that this type of injection can have only a limited efficiency and also requires maintaining high gas pressures on the order of 10^{-4} Torr (MO88) in the trap cavity to be effective.

Pulsed ion production has become conveniently accessible with the wide availability of high powered pulsed lasers. Using the LD technique a Pulsed Laser Ion Source (PLIS) can be produced in short bursts of ~ 100 ns width (BR86). The timing of the pulses is controlled by the laser firing and can be synchronised with the RF phase of the trap. Because of the small percentage of the cycle during which efficient trapping is possible the cyclical nature of the PLIS

makes it ideally suited as an ion source for injection into an RFQ trap. Furthermore there is a naturally occurring separation of different mass groups in transporting a pulsed source because of the different flight times. This offers a selective injection mechanism since only one mass is available for capture at any given time.

Injection of ions from a PLIS into an RFQ trap was attempted by Louris et al. (LO89). Ions were desorbed from a target a few centimetres away from the trap and injected through an aperture in one of the endcap electrodes. However, the advantages of this type of injection were not made obvious in their results. The proximity of the ion source to the trap made it impossible to control the purity of the injected sample beyond a certain m/z cutoff which they referred to as the "exclusion limit." There was still evidence that ions with an m/z value above this limit as well as neutral particles were also able to gain assess to the trap cavity. This work also relied on inter-ion collisions or collisions with a buffer gas to reduce the kinetic energy of injected ions. They did not report on the efficiency of their method.

It was the undertaking of this thesis to investigate the feasibility of mass-selective injection of externally created ions into an RFQ trap. The approach was novel in that a Time Of Flight (TOF) selection mechanism ensures the purity of the captured ions. No buffer gas was employed in this work and ion capture did not rely on collisions to reduce the kinetic energy of injected ions. As an alternative, an electric retarding potential was employed and the efficiency of this method was also investigated.

The work is presented in the following manner. In Chapter II of this thesis the theory of the Paul trap and ion injection is presented. A description of the experimental apparatus employed for this work is supplied in Chapter III. Chapter IV presents and discusses the results while conclusions derived from the experiments are presented in Chapter V.

Chapter II

Background Theory

2.1) Introduction

An RFQ trap consists of three electrodes, a ring and two endcaps. A radio frequency potential (RF) applied to the ring relative to the endcaps produces an oscillating quadrupole field inside the trap cavity. The periodic nature of the field produces 3-dimensional alternating restoring forces which affect ions deviating from the center of the trap cavity. Not all ions will be stable for a given field and solutions for stable ion motion will define the trapping conditions. From the equations for stable ion motion a 3-dimensional pseudopotential well that models the trapping mechanism is derived.

The amplitude of the RF field can be quite high for practical trapping conditions, typically on the order of several hundred volts. The varying field conditions of the trap create difficulties for injecting externally created ions. The RF phase of injection and the ion energy are both factors affecting the ion capture capabilities of the RFQ trap.

This chapter is divided into two sections that examine the basic theory of the RFQ trap and the conditions for ion injection. The theory of ion confinement is examined in Part I while the injection phenomena is examined in Part II.

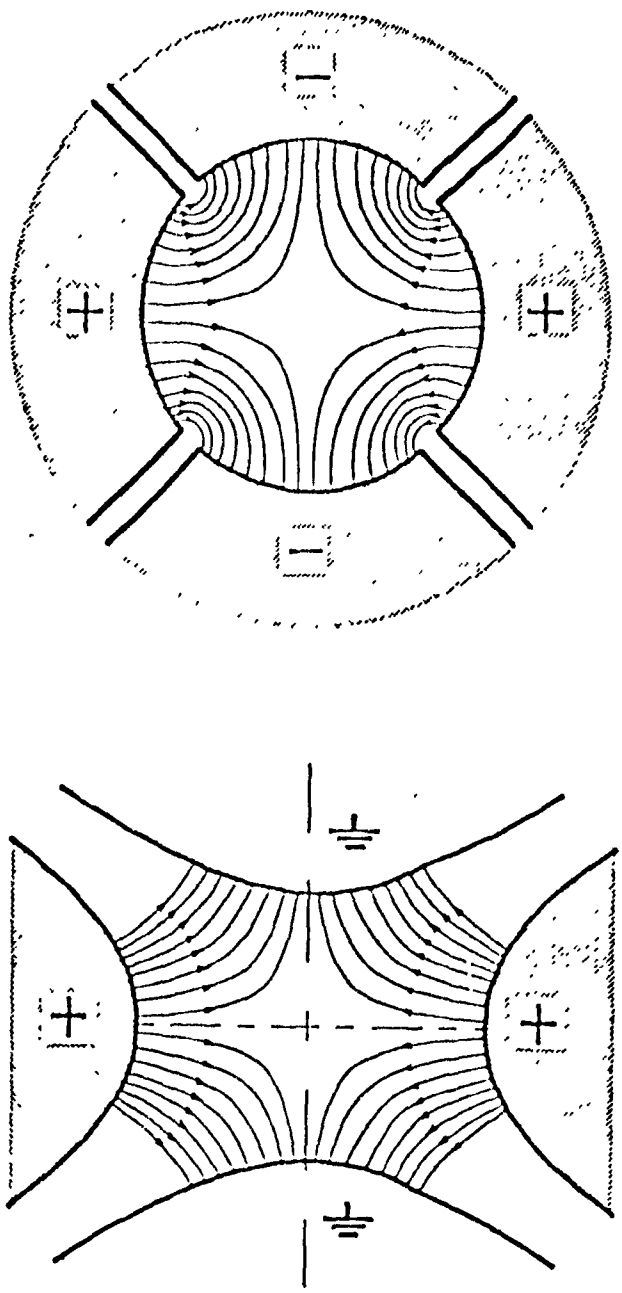

Figure 2.1: Two electrode configurations to produce a quadrupole electric field. Reproduced from (BOL90).

Part I: RFQ Trap

2.2) The Quadrupole Field

A quadrupole field is defined in cartesian co-ordinates by the equation

$$E = E_o(\lambda x+\sigma y+\nu z) \tag{2.1}$$

where λ, σ and ν are constants and E_o is independent of position. From this we observe that the strength of the field varies independently in each co-ordinate direction and is linearly proportional to the distance from the origin along each axis. Figure 2.1 is an example of a quadrupole field in 2-dimensions.

This field is subject to the constraints of Laplace's equation (assuming no free charges within the field region.)

$$\nabla \cdot E = 0 \tag{2.2}$$

Solving yields the following relationship

$$\lambda + \sigma + \nu = 0 \tag{2.3}$$

Any combination of values for λ, σ, and ν satisfying equation (2.3) will yield a valid solution for a quadrupole field defined by (2.1). The simplest form for an RFQ trap which requires confining the particle in 3-dimensions is of the form

$$\lambda = \sigma, \quad \nu = -2\sigma \tag{2.4}$$

The corresponding electric potential ,ϕ , to this field is obtained from the differential equation

$$E = \nabla \phi \tag{2.5}$$

Integrating (2.5) to solve for ϕ yields a solution of the form

$$\phi = \phi_o \lambda (x^2 + y^2 - 2z^2) \tag{2.6}$$

or in cylindrical co-ordinates

$$\phi = \phi_o \lambda (r^2 - 2z^2) \tag{2.7}$$

The electrode geometry to support this potential with three dimensional rotational symmetry, confining a particle in all directions, is seen in figure 2.2. It consists of a cylindrical ring enclosed at either end by two endcaps. The inner surface of the ring and endcaps follow the form of two complimentary hyperbolas when viewed in the rz cross-section. The inner radius of the cylinder is defined as r_o and the perpendicular distance between endcaps as $2z_o$.

Given the diameter of the ring as $2r_o$ one can solve (2.7) for λ.

$$\lambda = \frac{1}{2r_o^2} \tag{2.8}$$

and following from that establish the relation

$$r_o = \sqrt{2} z_o \tag{2.9}$$

The final form of the RFQ trap potential in cylindrical co-ordinates is then

$$\phi = \phi_o \frac{(r^2 - 2z^2)}{2r_o^2} \tag{2.10}$$

Other solutions to equation (2.3) will yield quadrupole fields with different electrode geometries.

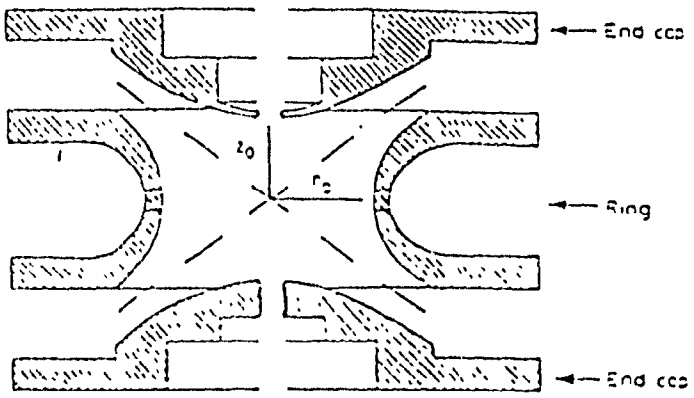

Figure 2.2: Electrode geometry to support a 3-dimensional rotationally symmetric quadrupole potential. The inner surfaces of the ring and endcap electrodes are complimentary hyperboloids. Reproduced from (DA76).

As an example, for

$$\lambda = -\sigma = \frac{1}{2r_o^2}, \quad \nu = 0 \tag{2.11}$$

one obtains the potential for the quadrupole mass filter. The related electric fields confine the particle in only two dimensions.

2.3) Equations of Motion

Under normal RFQ trapping conditions both DC and AC components may be present. Then

$$\phi_o = U - V\cos\omega t \tag{2.12}$$

where $V\cos\omega t$ is the AC RF potential applied between the ring and endcap electrode to form the quadrupole field while U is a DC component which can be superimposed on the ring to alter the stability characteristics of particles in the trap, (refer to section 2.5 for further explanation.) Substituting, equation (2.7) then takes on the form

$$\phi = (U - V\cos\omega t)\frac{(r^2 - 2z^2)}{2r_o^2} \tag{2.13}$$

One obtains the corresponding electric field equations from (2.5)

$$E_r = -\frac{\delta\phi}{\delta r} = -(U - V\cos\omega t)\frac{r}{r_o^2} \tag{2.14}$$

$$E_\theta = -\frac{1}{z}\frac{\delta\phi}{\delta\theta} = 0 \tag{2.15}$$

$$E_z = -\frac{\delta\phi}{\delta z} = (U - V\cos\omega t)\frac{z}{2r_o^2} \tag{2.16}$$

The equation of motion of a singly charged particle in the influence of an electric field is given in one dimension by

$$-eE_x = m\frac{\delta^2 x}{\delta t^2} \qquad (2.17)$$

where e is the electron charge and m is its mass.

Substituting for E_r and E_z we obtain the equations of motion for the particle in the 3-dimensional rotationally symmetric electric quadrupole field of an RFQ trap in cylindrical co-ordinates.

$$\frac{\delta^2 r}{\delta t^2} - \frac{e}{mr_o^2}(U - V\cos\omega t)\, r = 0 \qquad (2.18)$$

$$\frac{\delta^2 z}{\delta t^2} - \frac{2e}{mr_o^2}(U - V\cos\omega t)\, z = 0 \qquad (2.19)$$

One observes that motion in the r and z directions is independent and one may treat each case separately.

2.4) Mathieu Equations and Solutions

Equations (2.18) and (2.19) are of the Mathieu type and may be expressed in the canonical form of the Mathieu equation

$$\frac{\delta^2 u}{\delta \xi^2} + a_u - 2q_u\cos 2(\xi - \xi_o)\, u = 0 \qquad (2.20)$$

by making the following transformations

$$u = r,\ z \tag{2.21}$$

$$\xi = \frac{1}{2}\omega t,\ \xi_o = \frac{1}{2}\omega t_o \tag{2.22}$$

$$a_z = -2a_r = -\frac{4eU}{mz_o^2\omega^2} \tag{2.23}$$

$$q_z = -2q_r = -\frac{2eV}{mz_o^2\omega^2} \tag{2.24}$$

Solutions to this second order differential equation can be expressed by

$$u = \alpha' e^{\mu\xi} \sum C_{2n} e^{-2\epsilon\xi} + \alpha'' e^{-\mu\xi} \sum C_{2n} e^{-2\epsilon\xi} \tag{2.25}$$

where α' and α'' are integration constants dependent on the ions initial conditions of position, velocity and RF phase at time $t = t_o$ when the ion is first subject to the quadrupole field. The coefficients C_{2n} and μ are constants representing the amplitude of oscillations and the frequencies of the infinite number of components respectively. Both depend only on the values of the parameters a and q from which they may be calculated using a series of recurrence relations in the form of continuous fractions (MA90), they are independent of the initial conditions.

A stable solution is defined as one where the particle remains within the cavity of the trap indefinitely, that is for $r < r_o$ and $z < z_o$. From (2.25) we observe that the governing variable of motion is μ and the stability of the ions in the trap will depend directly on the value assigned to it. Note that since μ is dependent solely on the parameters a and q all ions with the same (a,q) value will exhibit the same periodicity of motion.

There are four possible forms of solutions for the value of μ:

(1) μ is real and non-zero

The $e^{\pm\mu r}$ terms diverge rendering this solution unstable.

(2) $\mu = (i\beta + \alpha)$, μ is a complex number

These solutions are also unstable, the $e^{\pm\alpha}$ behaving in a manner similar (1).

(3) $\mu = i\beta$, μ is purely imaginary and β is an integer

These solutions are periodic but unstable.

(4) $\mu = i\beta$, μ is purely imaginary and β is not an integer

These solutions are both periodic and stable.

One then assumes a solution of the form of (4). From equation (2.25) one can visualize the resulting ion motion. It will exhibit a low frequency "secular" motion with a period of $1/\beta$ on top of which the higher frequency RF "micromotion" is superimposed. An example is depicted in figure 2.3. The parameter u however is representative of both the r and the z directions. The ions therefore possess both radial and axial components of this motion and there are two respective fundamental frequencies determined by β_r and β_z. These fundamental frequencies are defined by

$$\Omega_{r,z} = \frac{\beta_{r,z}\,\omega}{2} \qquad (2.26)$$

Solutions for β are obtained from a complicated relationship dependent on the parameters a and q, see (DA76). There are many approximate solutions, one commonly used (DA76) form is the following

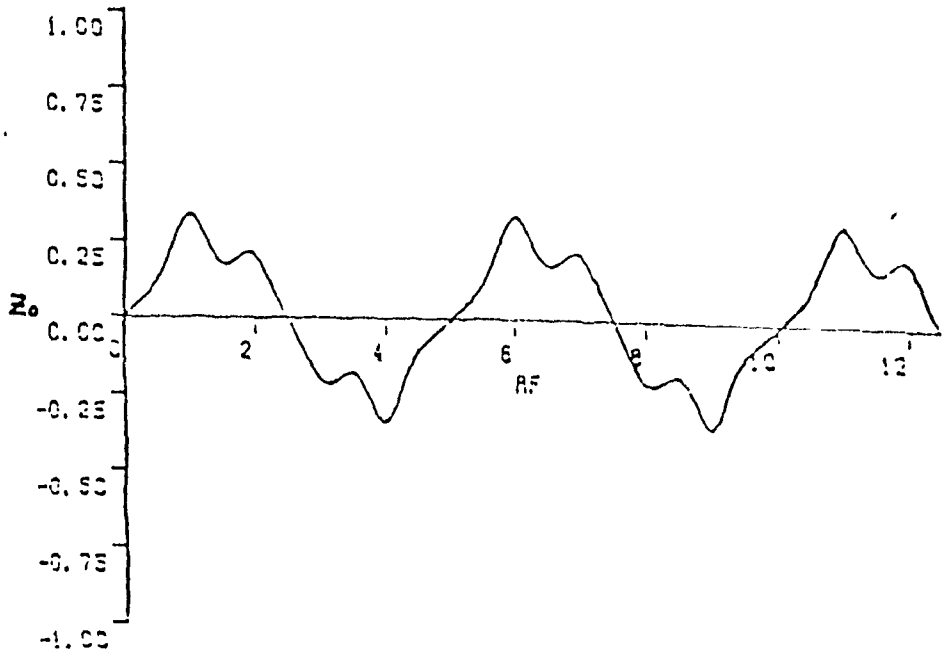

Figure 2.3: Simulation of oscillatory motion of ion along the z-axis in an RFQ trap. Reproduced from (LUBE

$$\beta = \sqrt{(a+\frac{q^2}{2})} \qquad (2.27)$$

2.5) The Stability Diagram

The constraints on β for stable solutions allows one to establish a closed set of (a, q) values. A plot of these parameters is known as a stability diagram. It is shown in figure 2.4 for both the r and z co-ordinates.

For 3-dimensional confinement, as is the requirement of the RFQ trap, motion must be stable in both the r and z directions. This can be achieved only by operating in the overlapping stability zones of the (a_r, q_r) and the (a_z, q_z) stability diagrams. Though any of the overlapping regions will yield stable solutions for most work with the RFQ trap is limited to the first stability zone where a and q are both small. An enlarged view of this region is presented in figure 2.5, it is known as the "Mathieu stability diagram."

A trapped particle must possess an (a,q) co-ordinate that lies on the Mathieu stability diagram to be confined indefinitely in an RFQ trap. Ions whose (a,q) co-ordinates do not lie within the boundaries of the diagram are "unstable" in the field and can only remain in the trap for a finite period, their movement eventually exceeding the limits of the trap cavity.

Recall from the definitions of the parameters a and q (equations (2.18) and (2.19) respectively) that they are dependent on U, V *and* ω for a given ion and trap geometry. Thus the physical implications of the diagram are that a particular ion can be trapped indefinitely only over a limited range of these values. For example, given the trap geometry of this work, an AC potential of 360 V at 650 kHz and no DC component the lightest mass singly charged ion that possesses an (a,q) co-ordinate within the bounds of stability is 23 amu, all heavier masses are stable. The addition of a positive DC component to the ring will shift the a co-ordinate

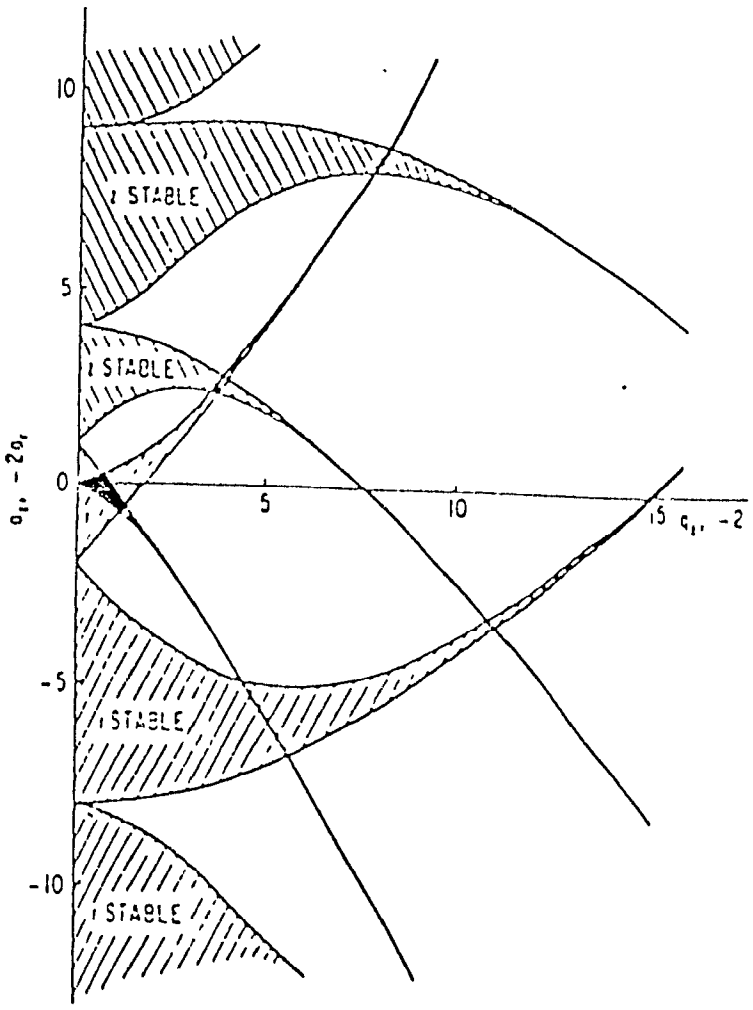

Figure 2.4: Superimposition of r and z stability diagrams The first common rz stability region has been inked in for clarity. Reproduced from (DA76)

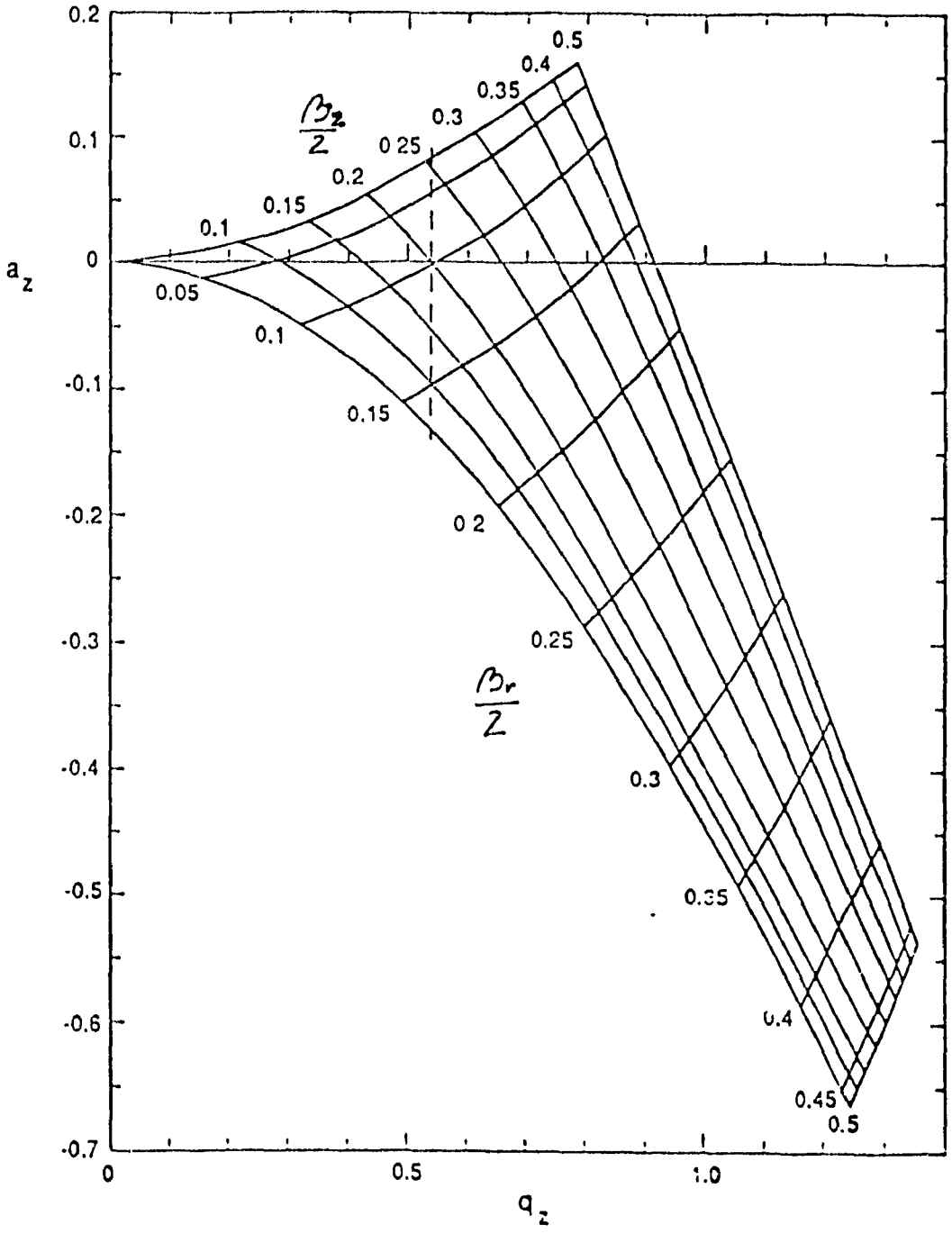

Figure 2.5 Enlargement of first rz stability region, known as the "Mathieu Stability Diagram." Reproduced from (M091).

down, for 20 V DC masses as light as 20 amu are now stable. Reducing the value of V will shift the q co-ordinate towards the origin , for V equal to 300 V ions with a mass greater than 50 amu no longer have stable (a,q) co-ordinates. This is the basis for mass selective ejection of ions, by varying any of U, V or ω the co-ordinates a and q are shifted beyond the limits of the stability diagram and the undesired masses are eventually ejected from the trap.

2.6) Pseudopotential Well

Since the ion's β value will contribute to its overall energy it will be a factor in determining how long the unstable ions are allowed to oscillate before they are lost. By the same token it will be a factor in determining the extent to which "stable" ions can be confined, that is to say, how much kinetic energy an ion with a stable (a,q) co-ordinate can possess and yet still be unable to escape the trapping field. Since values for β vary with (a,q) over the stability region some will be favoured over others for confining particles.

It was shown by Dehmelt (DE67) that the energy of the β oscillation can be thought of as an oscillation in a pseudopotential well. The depth of the well is calculated from the maximum oscillation energy of an ion can possess while fulfilling the (a,q) stability requirements. In the axial direction this is given by

$$D_z = \frac{m}{8}\beta^2\omega^2 z_o^2 \qquad (2.28)$$

By making the transformations defined in equation (2.9) the corresponding potential well in the radial direction is found.

$$D_r = \frac{m}{16}\beta^2\omega^2 z_o^2 \qquad (2.29)$$

The shapes are paraboloid; the depth is proportional to the square of the distance from the origin (see tables 2.1 and 2.2 for examples of the well depths for various cases). Figure 2.6

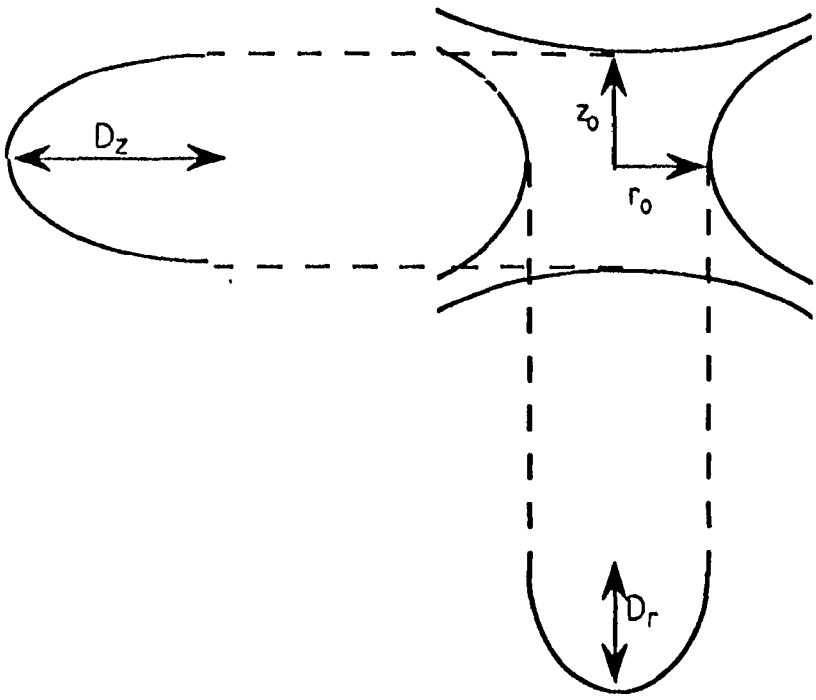

Figure 2.6: Potential well depth in axial and radial directions.

demonstrates the variation of the well depth in the axial and radial directions. Trapped particles are assumed to exhibit simple harmonic motion, oscillating in the 3-dimensional well.

2.7) Present Working Conditions

This work studied the injection and trapping of two different ions, the C_2^+ and C_3^+ ionic clusters of mass 24 amu and 36 amu respectively. Since only one mass at a time was captured no allowance for mass selective ejection was required and for simplicity, work was limited to the $a = 0$ line of the Mathieu stability diagram, (see figure 2.5). An AC potential of 360 Volt and 650 KHz was employed. This corresponded to a q value of .85 for a mass 24 ion and .55 for a mass 36 ion, both of which are in the region of stability. Though not necessarily providing the optimum trapping conditions for either mass, this particular choice gave satisfactory results for both and enabled alternate confinement of either the C_2^+ or the C_3^+ ions without requiring any adjustments to the field. Tables 2.1 and 2.2 present typical values of q, Ω_z, Ω_r, D_z, *and* D_r for both ions over a small range of amplitudes about 360 V for a 650 kHz AC potential.

Table 2.1: Various Trapping Parameters for a C_2^+ Particle Typical of Experimental Conditions[1].

V, (V)	q_z	D_z, (eV)	D_r, (eV)	Ω_z, (kHz)	Ω_r, (kHz)
280	.68	24	12	155	78
300	.73	27	14	166	83
320	.77	30	16	177	89
340	.82	34	18	188	94
360	.87	39	20	200	100
380	.91	44	22	211	105
400	*	*	*	*	*
420	*	*	*	*	*
440	*	*	*	*	*

*: $q > 0.91$, unstable configuration

Table 2.2: Various Trapping Parameters for a C_3^+ Particle Typical of Experimental Conditions[1].

V, (V)	q_z	D_z, (eV)	D_r, (eV)	Ω_z, (kHz)	Ω_r, (kHz)
280	.45	16	8	103	52
300	.48	18	9	111	56
320	.52	21	10	118	59
340	.55	23	12	125	63
360	.58	26	13	133	67
380	.61	29	14	141	70
400	.65	32	16	148	74
420	.68	35	18	155	78
440	71	40	20	163	82

(1) The RF potential has a frequency of 650 kHz, there is no DC potential therefore $a_z = 0$.

Part II: Injection Theory

2.8) Introduction

It was calculated by several different models that the capturing property of the RFQ trap is strongly dependent on the energy and RF phase angle of the ion at injection. Furthermore that no injected ion can remain trapped indefinitely unless its kinetic energy is reduced once inside the trap. That is to say, the trajectories of injected ions satisfying the initial energy and phase requirements eventually surpass the limits of r_o or z_o.

The problem of injecting externally created ions into an RFQ trap is then two-fold: ions must have sufficient kinetic energy and arrive within a limited RF phase angle to be injected into a "stable" orbit but they must subsequently lose some of that kinetic energy to remain trapped. The two principles of injection theory are examined separately: the energy and phase dependence of injection and the cooling of trapped ions.

2.9) Retardation Factor

The dependence of the confinement of ions on their kinetic energy is easily understood in terms of a potential well. Ions with kinetic energies greater than the pseudopotential well depth defined by its (a,q) co-ordinates will not be confined by the trapping potentials. However injected ions must possess a minimum kinetic energy at any given RF phase just to gain access to the trap cavity and the greater the kinetic energy of the injected ion the less probable its confinement.

Figures 2.7a and 2.7b illustrate two injection scenarios. In figure 2.7a a particle with a net kinetic energy KE is injected into the well and it subsequently escapes. In figure 2.7b the kinetic energy is removed and it is subsequently unable to escape the well and remains trapped. Thus some mechanism for removing a part of the ions initial kinetic energy is required in order for them to succumb to the trapping potentials once in the trap cavity.

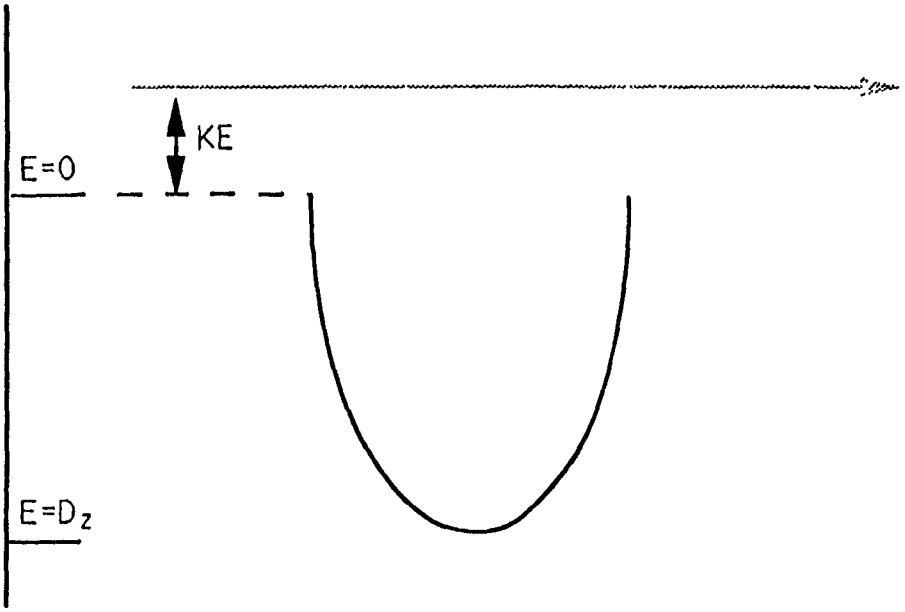

Figure 2.7a: Schematic of energy of injected ion in the axial direction. The ion escapes the potential well.

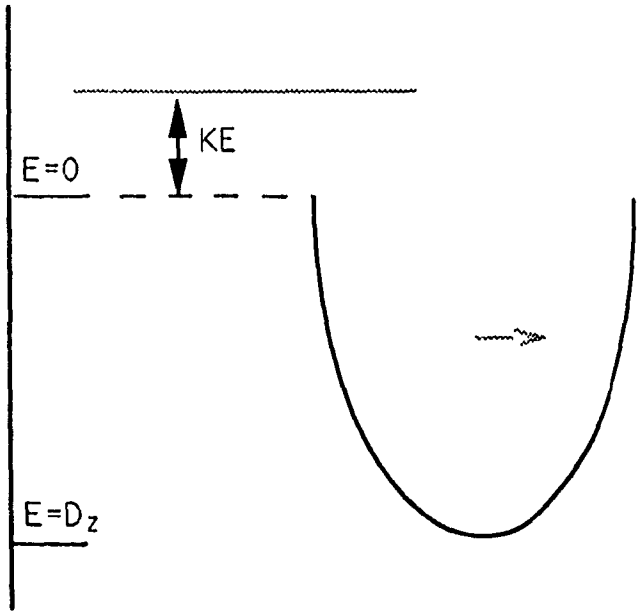

Figure 2.7b: Schematic of energy of injected ion in the axial direction. Some of the ions initial kinetic energy is removed and it remains trapped in the potential well.

Previous work with external sources and RFQ traps relied on collisions, usually with a light buffer gas, to cool the injected ions. As an alternative this work employed electrical retardation to reduce their kinetic energy. The principle is as follows. An ion subject to an electric potential over a period of time will receive an impulse resulting in a change of its momentum. A change in momentum translates to a change in kinetic energy.

An impulse (I) is defined by

$$I = \int F\,dt = \Delta p = \int m\,dv \qquad (2.30)$$

here F is the force acting on the particle, Δp is the change in momentum of the particle, m is its mass and v is its velocity.

To reduce the kinetic energy of an injected ion an opposing retarding pulse can be applied. In this work the pulse is imposed by dropping the potential on the "entrance" endcap with respect to the other electrodes as the ions enter the cavity.

The force F acting on the particle in an electric field can be calculated from the energy gradient. In the axial direction it is given by

$$F = q\frac{dV}{dz} \qquad (2.31)$$

The momentum of the ion after the impulse is

$$p_f = p_i - q\int \frac{dV}{dz}\,dt \qquad (2.32)$$

The final energy is then

$$E_f = \frac{p_f^2}{2m} \qquad (2.33)$$

Thus travelling through the retarding electric field reduces the ions' kinetic energy and enables their trapping. The final energy of the ion must be less than or equal to the pseudopotential depth of its (a,q) co-ordinate for efficient confinement of ions.

2.10) Injection Energy and Phase Dependence

The simultaneous dependence of the energy and time of arrival of the ions with respect to the RF phase on their trapping potential lends strongly to the application of a "phase-space" treatment to the analysis. This method is commonly used in the study of traps and trapping conditions.

Phase-space is a six-dimensional co-ordinate system defined by the parameters (x,y,z) and (p_x,p_y,p_z) representing position and momentum vectors respectively. A phase-space "volume" specifies a closed set of these vectors at any time t. It is a property of the Mathieu equation that only ions occupying a specific phase-space volume possess stable orbits. It can be seen indirectly from equation (2.20) that for stable motion the simultaneous values of u and u' are dependent on the RF phase ξ and that the phase-space acceptance of an injected ion is a direct result of the dependence of u and u' on the initial phase ξ_o. The simultaneous position $\mathbf{u(t)}$ and the momentum $\mathbf{u'(t)}$ of an injected ion must fall on or within a phase-space volume, for any phase ξ, for the particle to be admitted to a stable orbit.

Conventional phase-space treatment employs the parameters of momentum and position. An energy and time co-ordinate for classical particles in the absence of any external forces can be expressed as a position and momentum co-ordinate by making the following transformations

$$p_i = \frac{\sqrt{2\,(KE)_i}}{m}, \quad i = t\frac{p_i}{m} \tag{2.34}$$

where i represents any of the co-ordinates x, y or z, m is the mass of the particle, KE is its kinetic energy and p is its momentum.

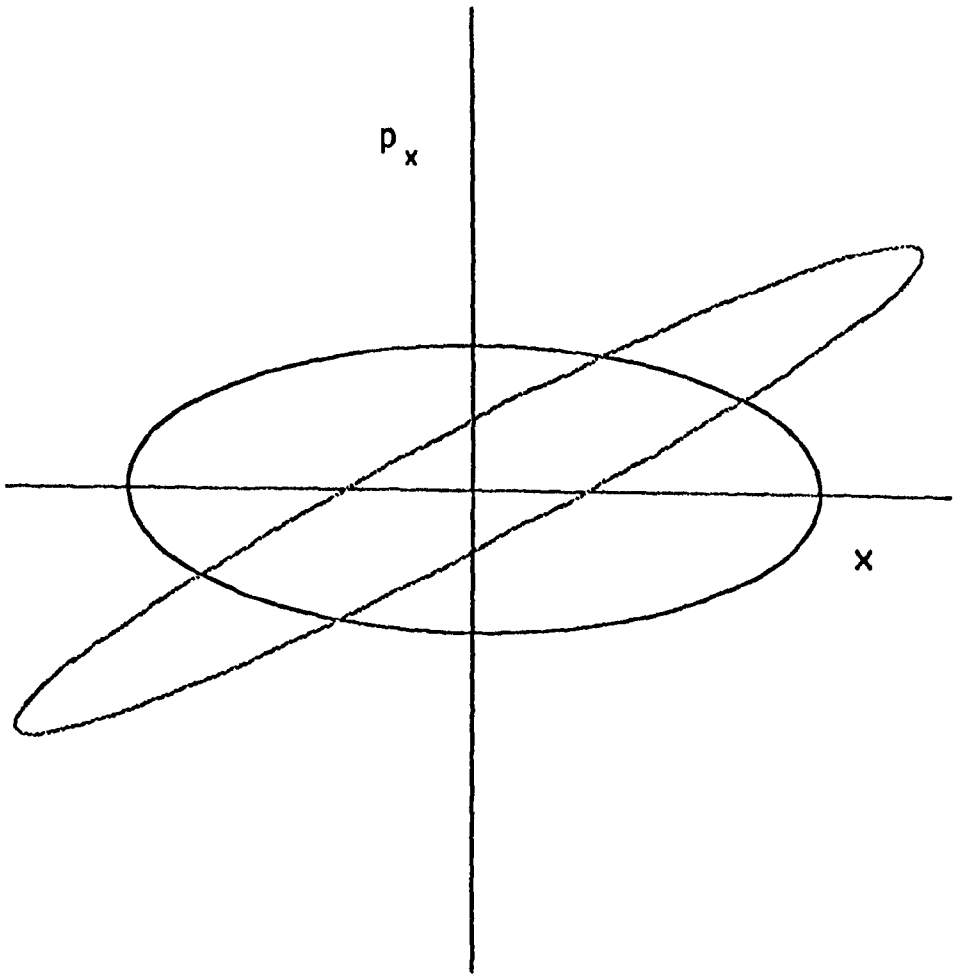

Figure 2.8: Phase-Space Ellipse
Projection of phase-space volume on the x and p_x axis at two different times.

The phase-space analysis exploits an elliptical relationship between x and **p** for a given ξ. In two-dimensions this appears as

$$\Gamma x^2 + Axp_x + B(p_x)^2 = \epsilon \qquad (2.35)$$

where Γ, B and A are constants dependent on the RF phase ξ and determine the orientation of the ellipse, see figure 2.8. The parameter ϵ is called the emittance, it is independent of ξ and defines the area of the ellipse. For an injected ion to be trapped its (x,p_x) co-ordinates must lie on or within the boundaries of this ellipse.

Recall the definition of a "stable" orbit was one where the ion's (a,q) co-ordinate lay on the Mathieu stability diagram and it could be trapped indefinitely. However a further criterion for stability is now applied, there is only limited phase-space volume inside the trap available to a stable ion. The shape of the "stability" ellipse varies though the absolute volume is constant over time. Even ions possessing stable (a,q) co-ordinates will be unstable in the field unless their (x,p) co-ordinates lie within the "stable" phase-space volume of the trap. An example of such an ion would be one injected into the trap, where the fields have been tuned such that the (a,q) co-ordinates of that mass are stable, with a large amount of kinetic energy. Such an ion would not be captured by the potential.

Figure 2.9 represents the "stable" phase-space volume along the axial direction of the trap at a certain time. The solid band above the ellipse is representative of a DC ion beam passing through the centre of the trap along the z-axis. Through collisions inside the trap, ions from the beam may change their position or momentum and alter their phase-space co-ordinates to lie inside the ellipse. These ions could then be trapped indefinitely. This is the conventional method for ion capture in RFQ traps where a light neutral buffer gas is usually employed for collisions. Of course the limitations of such a method are obvious, the collisions and phase-space shifts of the ions are random and the capturing efficiency is very low.

In figure 2.10 the injected beam is from a pulsed source, it traverses the trap in a bunch. The effect of an efficient cooling mechanism is demonstrated. At a particular moment in time the

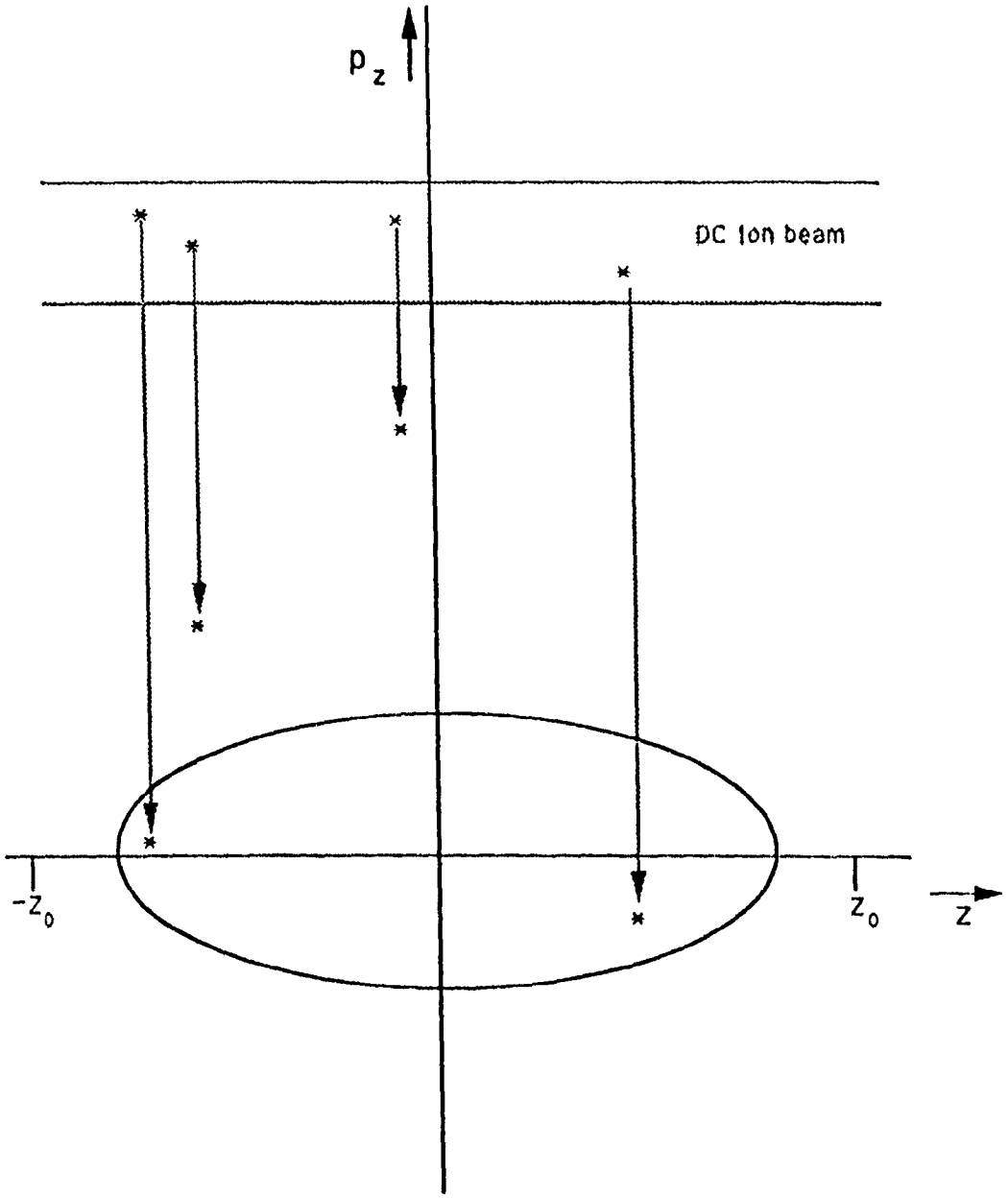

Figure 2.9: "Stable" phase-space volume of the trap and injected DC beam, at a particular time, projected on the z and p_z axes. Ions in the beam can undergo collisions inside the trap and shift their position in phase-space.

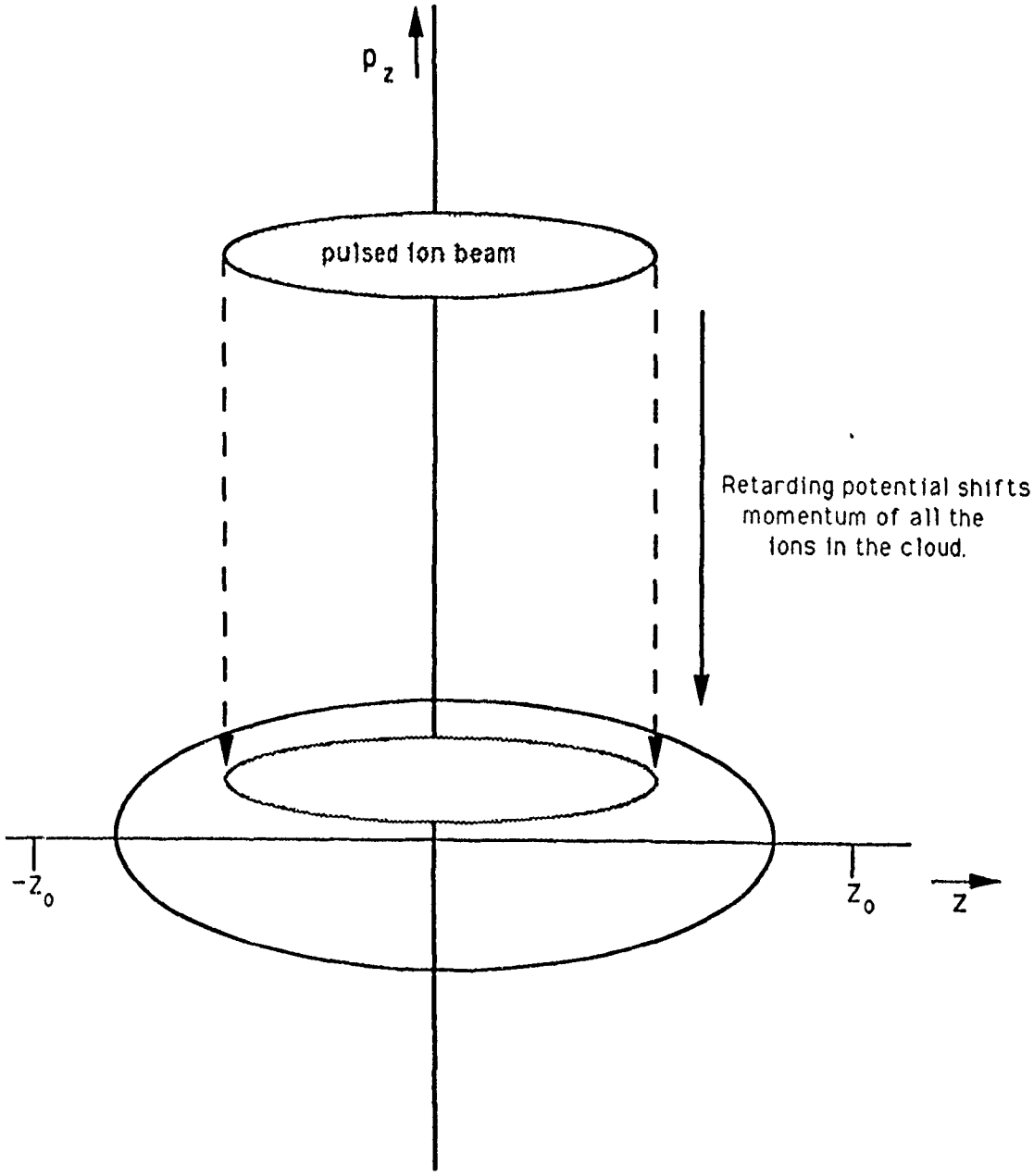

Figure 2.10: "Stable" phase-space volume of the trap and injected pulsed ion cloud, at a particular time, projected on the z and p_z axes. With an efficient retarding mechanism all the ions in the cloud can undergo a phase-space shift.

momentum of the entire cloud could be shifted to lie on the "stable" ellipse. Since the shape of the phase-space volume is periodic the efficiency of any systematic retarding mechanism will also be periodic.

Through the use of an electric retarding pulse described in section 2.9, this is exactly the technique proposed and investigated in this work. The cyclical nature of the pulsed beam and the effectiveness of the retarding potential are ideally coupled to effectively inject into an RFQ trap.

Chapter III

Experimental Apparatus

3.1) Experimental Method

The experimental apparatus used in this work is presented in figure 3.1. The specific functions of the apparatus may be divided into three main sections: Injection, Trapping and Detection.

Injection: The first section incorporates the ion source and injection mechanism. Ions were created by laser desorption at the target (#1) and transported to the "entrance" endcap (#7) for injection into the trap. During the transport period a TOF mass separation occurs which in turn enabled one to distinguish between various q/m groups in the source.

Trapping: The second section of the apparatus was occupied by the RFQ ion trap (#7, #8, #9) and its functions. The ions were introduced into the trap cavity through the "entrance" endcap. which also served to decelerate the targeted q/m ion cloud by applying a fast retarding pulse shortly after its entry. After a specified period of trapping had transpired the ions were removed from the trap by applying an extraction pulse on the "exit" endcap (#9).

Detection: The third section of the apparatus contained the extraction drift tube and detector.

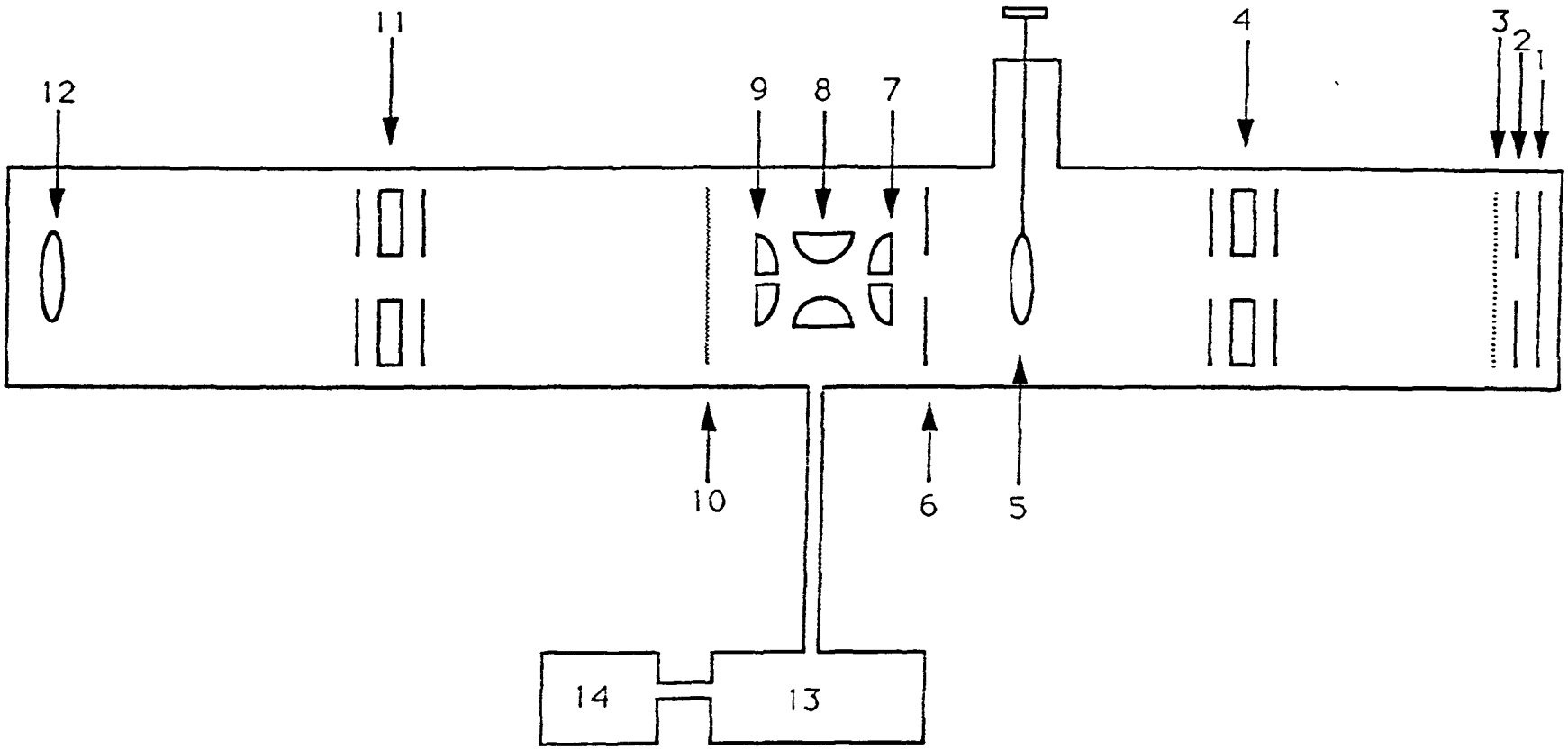

Figure 3.1: Layout of Apparatus

1) Target
2) Accelerating Plate
3) Grounded Screen
4) Einzel lens, E1
5) Retractable ChannelPlate Detector, D1
6) injection lens
7) "Entrance " Endcap
8) Ring Electrode
9)"Exit" Endcap
10) Grounded Screen
11) Einzel Lens, E2
12) Channel Plate detector, D2
13) Turbo Pump
14) Mechanical Pump

Upon extraction the ions were transported to the detector D2 (#12). The output of the detector was monitored on a digital oscilloscope and could be recorded.

The transport and ion-optics system was designed using the program SIMION developed by D.C. McGilvery (DA88). SIMION provided a graphic representation of the field potentials and ion trajectories through a user defined electrostatic system.

The experiments were conducted at a pressure of 2E-6 Torr. This value was sustained by a turbo molecular vacuum pump (#13) with mechanical backpumping (#14).

3.2) Injection

A) Laser Ion Source

The ions were created by pulsed laser desorption. This is a process which occurs when a laser beam irradiates a target and thermally excites particles. When sufficient energy has been provided they are ejected from the surface in a cloud. The variety of particles created includes atoms, clusters and molecules, both neutral and ionic depending on the target material and the focusing conditions of the irradiating beam. As a result of the desorption process the source possesses a net energy spread, the extent of which will vary with the intensity of the laser (BR86). The more energy provided by the laser, the larger the number of particles that are produced. The higher density of the source results in more numerous collisions and repulsive ionic interactions which causes broadening of the spatial and energy spreads.

An Nd:YAG pulsed laser was used for the desorption. The YAG had a fundamental wavelength of 1064 nm and a frequency-doubling crystal was employed to obtain a 532 nm wavelength for use in these experiments. For a wavelength of 532 nm the energy of the laser at the target was less than 1 mJ/pulse. The duration of the pulse was about 10 ns and the beam was tightly focused on the target surface. See figure 3.2 for a diagram of the laser use.

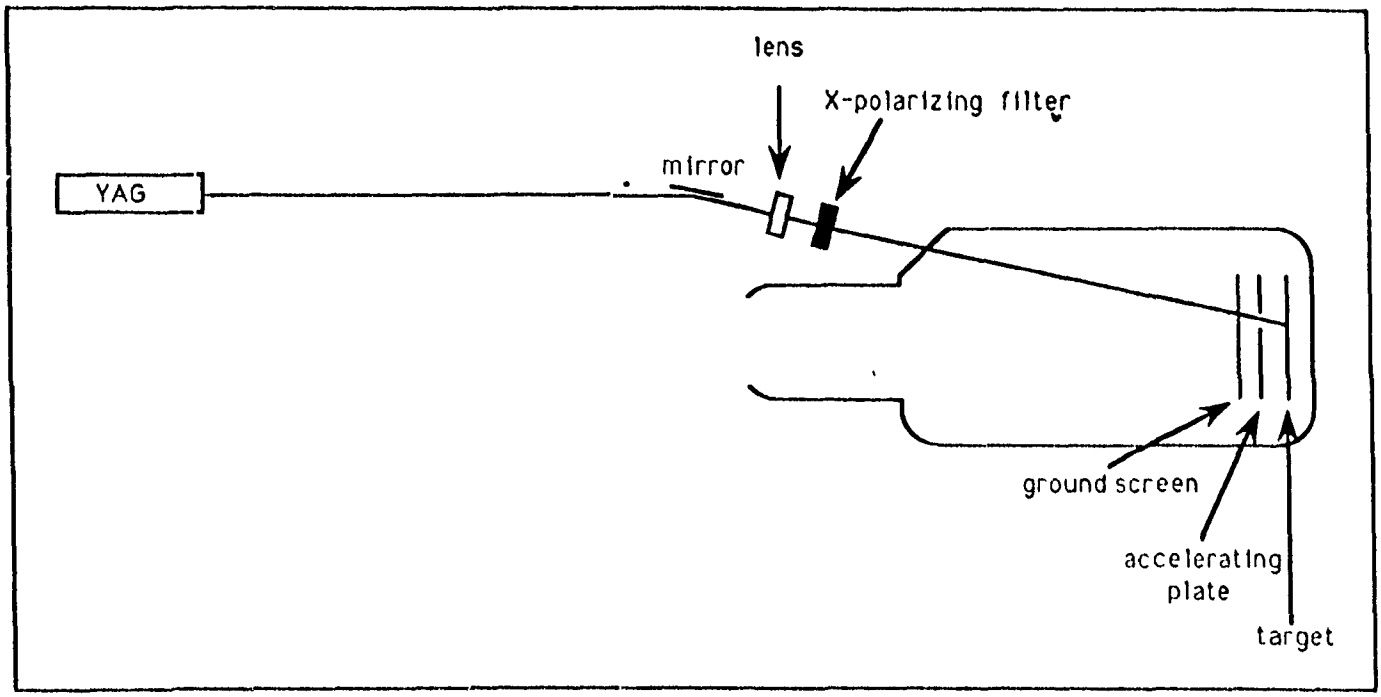

Figure 3.2: Ion production by laser desorption

B) Transport and Ion-Optics

Using SIMION, the transport and ion-optics system was designed to provide effective TOF mass separation and a tightly focused beam for transmission through the "entrance" electrode of the ion trap. Figure 3.3 is a simulation of the injection optics and transport system. The target and holder were kept at a 1 kV potential. Ions were created on the surface with a spatial spread of 5 mm which represented the possibility of a non-centred beam. An acceleration plate placed approximately 1cm from the target and directed the ions through a facing aperture. The potential on the plate was adjusted such that the diffraction caused by passing through the aperture is minimal. The first focus at A was a result of passing through the accelerating plate aperture. The ions then entered a field free region through a screened aperture on a grounded plate. The drift distance to the "entrance" endcap of the trap was 60 cm. The einzel lens E1 was located 25 cm from the target. Its potential was adjusted to collimate the beam along the axis of the flight tube into the injection lens. The effects of adjusting the accelerating plate and the einzel lens potential were monitored on the detector D1 which could be lowered into the beam path between E1 and the injection lens (see figure 3.3). The injection lens was located after D1, 10 cm from the "entrance" electrode of the trap. It was used to focus the beam so it could pass through the "entrance" endcap aperture and into the trap cavity. The potential was adjusted to focus the beam at B. The trap was kept at a potential of 910 V and ions were injected at 90 eV. The potential on the "entrance" endcap was then pulsed down to retard as they entered the trap.

C) Time of Flight Spectra

Figure 3.4 is a Time OF Flight (TOF) spectrum of a graphite source taken at detector D1. The timing of the two large peaks corresponds to the ionic clusters C_2^+ and C_3^+, their relative abundance was in agreement with other spectra for a Carbon PLIS (SE84). The small peak at 8.2 μs is believed to be a compound of the C_3^+ cluster. Since the principal ion group used in this work was the C_2^+ group the presence of the compound did not affect the conditions of the experiment and it was effectively ignored. It is the TOF separation of the C_2^+ and C_3^+ masses that enables them to be distinguished. This factor allowed one to trap each of the two masses

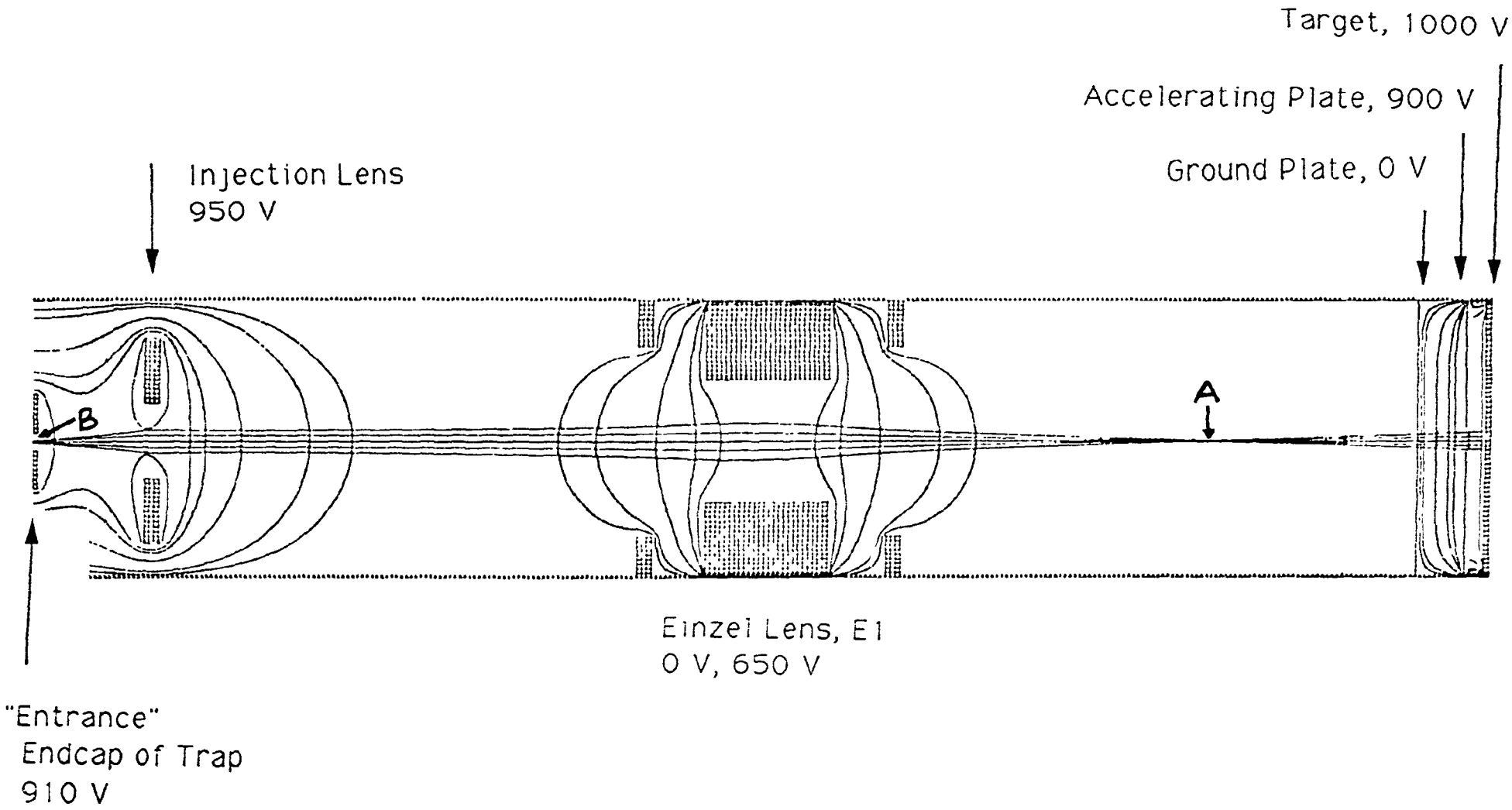

Figure 3.3: Injection Ion Optics

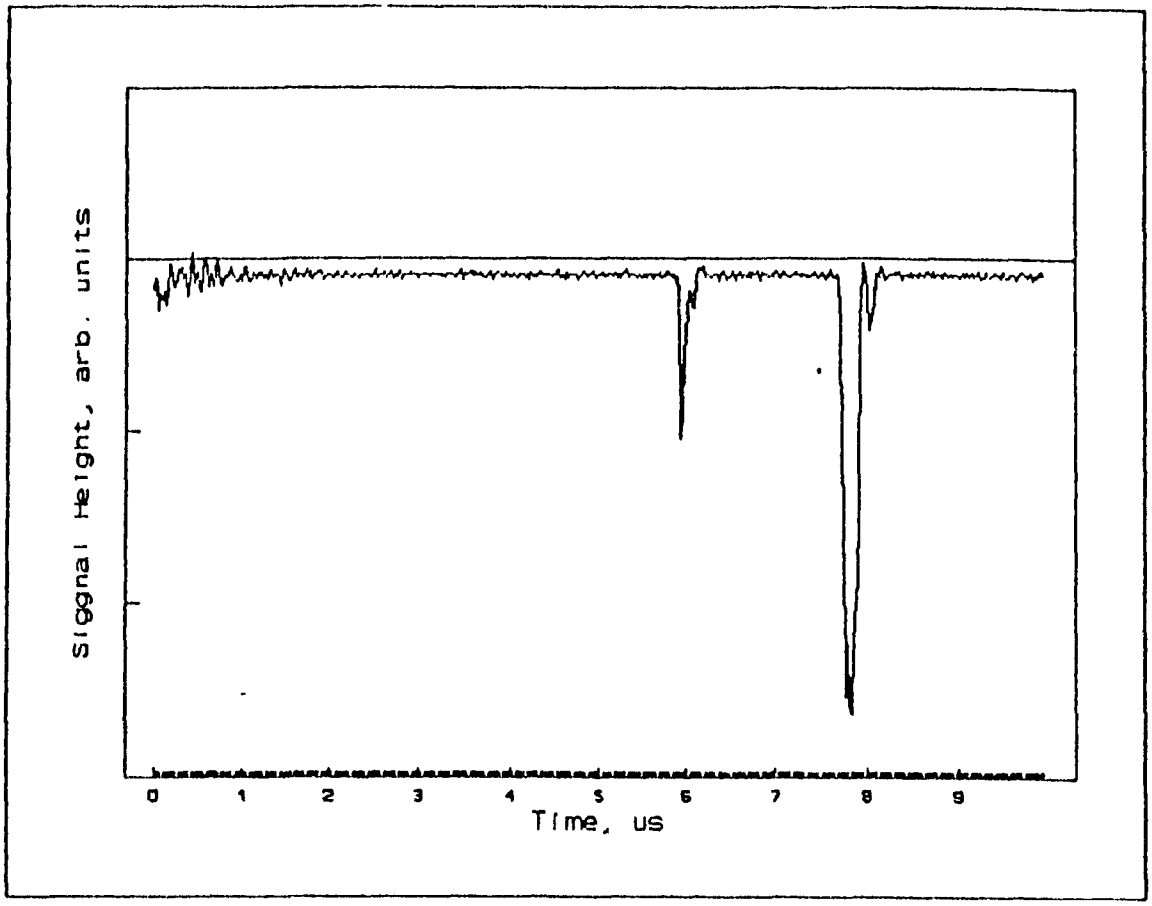

Figure 3.4: Time of Flight Spectrum of Graphite PLIS

separately. At D1 there was already a 2 μs lag between the peaks corresponding to a distance of approximately 15 cm at a transport energy of 1 keV.

The width of the peaks was the result of energy and spatial spreads in the clouds incurred in the desorption process. Because the C_2^+ peak was narrower it was used as the principle source for the experimental work presented in this thesis. The base of the C_2^+ peak is approximately 300 ns wide which corresponds to a spatial spread of over 2.5 cm. This spatial spread was a factor to consider when adjusting the timing and shape of the retarding pulse.

The lasers were triggered externally so the firing and hence, source creation, was synchronised with the RF phase of the ion trap. The laser output for each trigger is referred to as a "shot". The intensity of the irradiating beam and hence, abundance of the source, was controlled by a cross polarizing filter located near the target (see figure 3.2). A significant shot to shot variation of the source was observed and consequently spectra were taken over an average of 16 shots. Fresh surface areas were often contaminated and laser cleaning was required before a suitable spectra could be obtained.

3.3) Trapping

A) RFQ Trap

The RFQ trap used is made of stainless steel and shown in figure 3.5. As stipulated by the quadrupole field potential equation (2.7), the trap was designed so that equipotential surfaces of the ring and endcaps corresponded to complementary hyperbolae. The inner radius of the ring, r_o, is 2 cm and the corresponding distance between endcaps, $2z_o$, is 2.8 cm, in accordance with equation (2.9). See figure 3.5.

The endcaps each have a 1 cm hole in the centre. One, in the "entrance" endcap, is to allow the injection of ions from an external source. The other, in the "exit" endcap was used extract the ions from the trap at the other side. The extraction aperture is screened with an

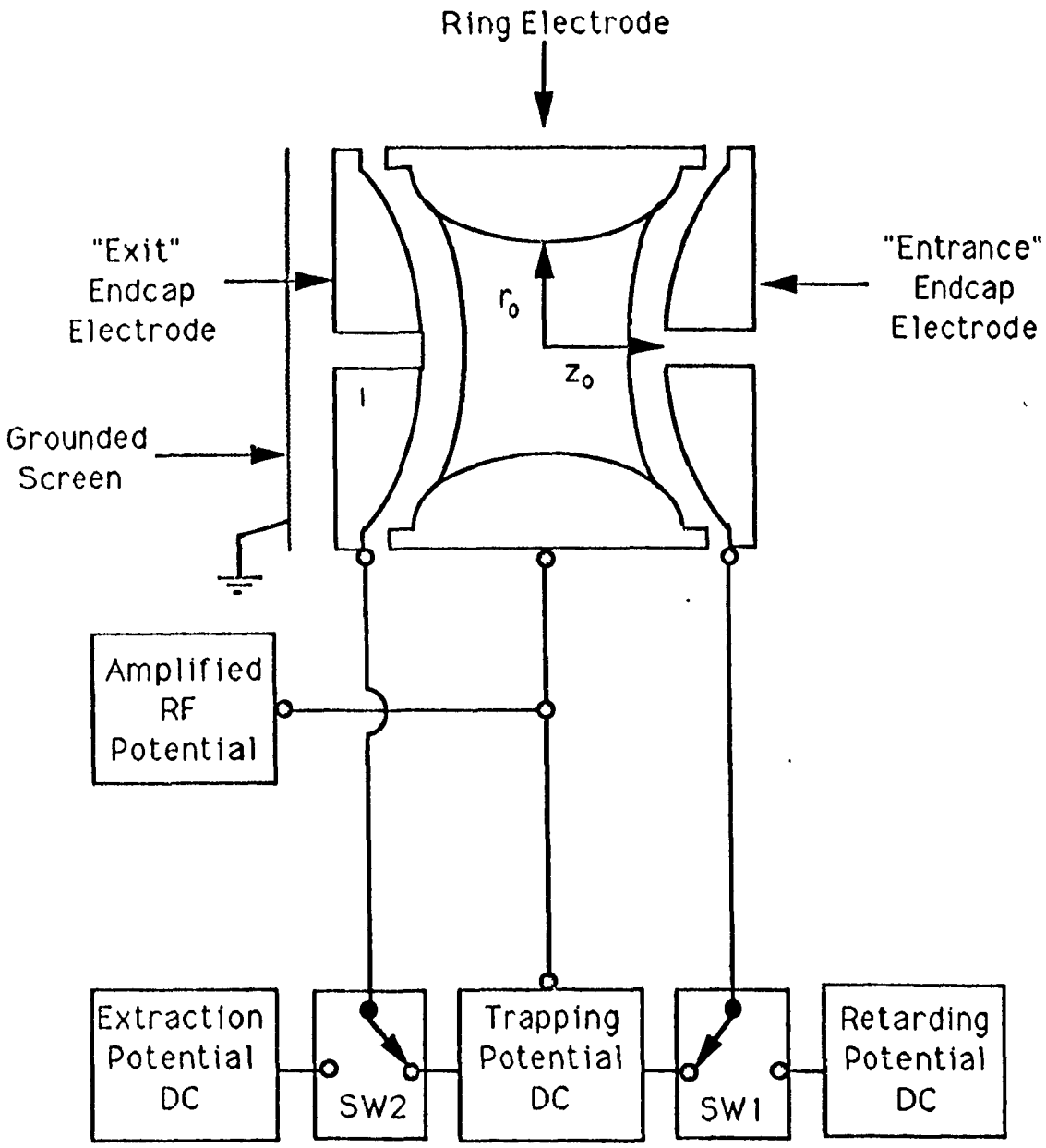

Figure 3.5: RFQ Trap Configuration

equipotential stainless steel mesh. The rationale for screening the "exit" opening was to minimise the diffraction of the extracted beam as a consequence of passing through the endcap aperture upon extraction. The influence of the "entrance" aperture on the ions was overshadowed by the strong fields from the retarding pulse and of the RF once inside the trap and this aperture was not screened.

There are four additional apertures on the trap which are located symmetrically about the central axis on the side of the ring. Though not of use for the bulk of the experiments presented in this work they were included in the construction of the trap to provide for spectroscopic and internal desorption experiments. Three of the apertures are of 0.5 cm in diameter, the fourth 1 cm.

Deviations from theoretical requirements in the physical assembly of the trap can affect the nature of the field inside the cavity. The topic is approached briefly here, a thorough analysis is available in (BO90). The effects of finite hyperboloid electrode surfaces, departures from true hyperbolic surfaces and apertures in the electrodes will introduce non-quadrupole components to the trapping field. To some extent they may be corrected by adding correction electrodes. A ring-like electrode sitting about the gap between the ring and endcap electrodes will help reduce the higher order components introduced by the finite electrode surfaces. The effects incurred by deviations from true hyperboloid surfaces are felt less near the centre of the cavity, their influences on the trapped ions can be reduced by increasing the dimensions of the trap. Finally, screening the apertures with equipotential mesh will lessen their higher moment contributions. High precision measurements would require taking such steps to maintain a pure-quadrupole field, however for the purpose of this work small deviations in the field can be neglected.

Under normal trapping conditions the ion trap sits at 910 V, 90 V below the target potential. Both endcaps could be pulsed to a lower DC potential as shown in figure 3.5. On the "entrance" endcap this feature is referred to as a "retarding" pulse and it was used to slow the ion cloud after it entered the trap. The "exit" endcap had an identical and independent pulsing feature, referred to as the "extraction" pulse. It was used to extract the trapped ions through

its central aperture.

B) Retardation

Ions were injected at 90 eV. For the most part this energy was directed in the axial direction with some radial components present due to the fanning of the focused beam. When the retarding pulse was applied the HV on the "entrance" endcap was connected to V_{re} and ions inside the trap were subjected to a retardation force. The retardation impulse opposed the kinetic energy of the fanned beam and slowed the ions inside the trap. The pulse height was such that it removed sufficient energy from the ions to enable their trapping and its width was short enough to affect only one q/m group of ions. Typical values were of the order of 150 V for 500 ns. The timing of the pulse was synchronised with the RF. Since there was a time width associated with the PLIS there was a certain RF phase angle over which the timing of the retarding pulse was effective.

Figure 3.6 is a simulation of the effect of a retardation force on ions injected into the trap. The ion trajectories started on the plane A with 90 eV kinetic energy and an angular divergence to match the injection conditions of figure 3.3. Ions were immediately subjected to a constant force produced by switching the "entrance" endcap electrode to a potential 100 V lower than the ring and "exit" endcap. The retarding effect may be observed by the converging spacing of the time markers on the ion trajectories as they enter the cavity. The retarding field eventually stops the ions which in this simulation were subsequently accelerated outside of the trap. The electrostatic limitation of the SIMION program did not allow the endcap potential to be pushed back up to normal trapping conditions and the constant retarding potential resulted in the reversal of the ion motion and their escape from the cavity through the same aperture. In practice the retardation potential was pulsed and the endcap was returned to a normal trapping potential before the ions were accelerated out of the trap. This simulation were also performed without an RF voltage. Though the RF field would have a strong influence on the phasing of the injection, the oscillatory nature of its influence would not result in any net energy loss for the injected ions. The assumption was that the RF effects could be superimposed onto the retarding

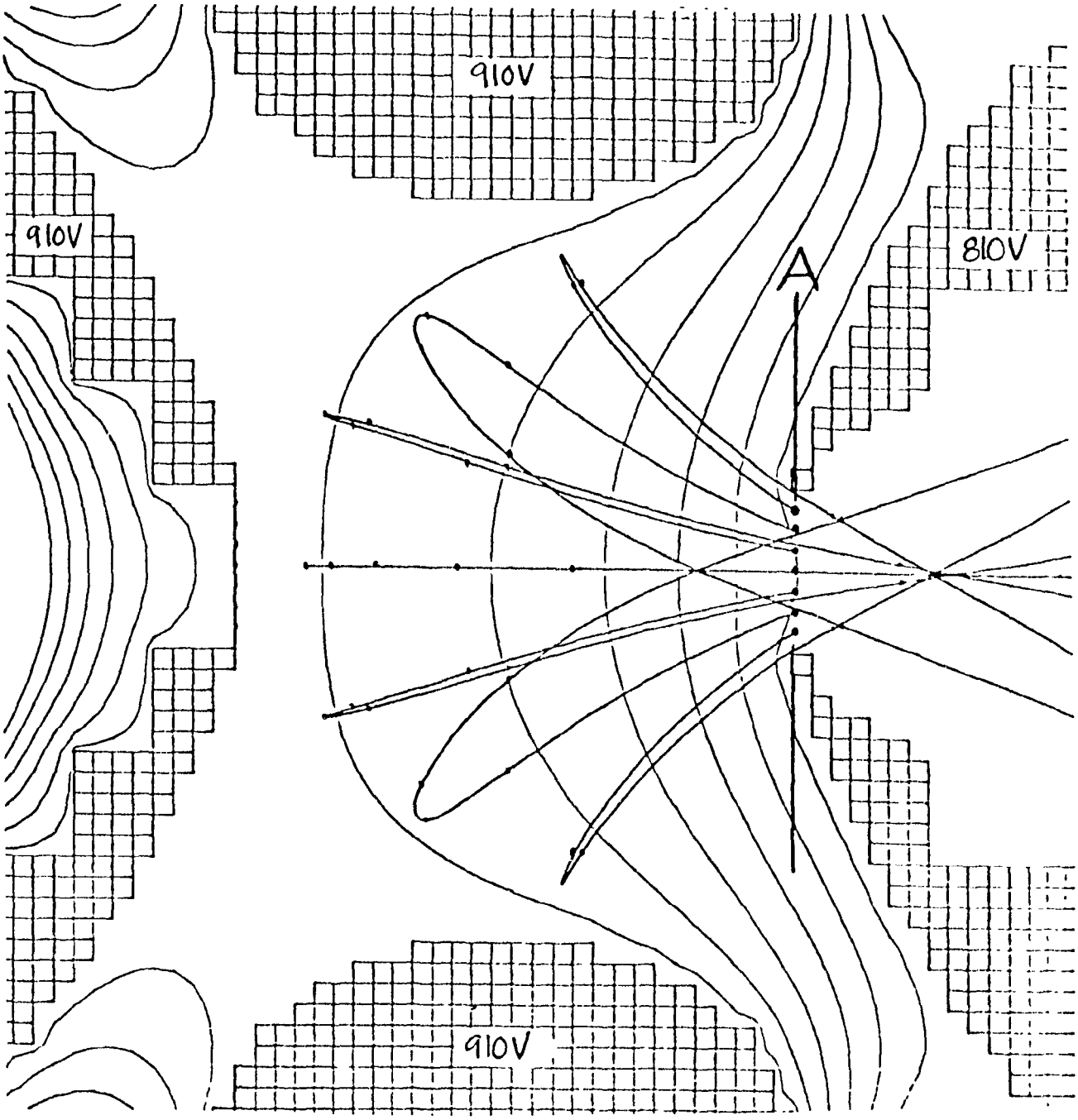

Figure 3.6: Simulation of ion motion inside the trap cavity under the influence of a retarding pulse. At t=0 the ions are located on the plane A with 90 eV kinetic energy and an angular divergence to match the injection conditions of figure 3.4. The dots on the ion trajectories are time markers, their spacing is 1 us. Observe the injected ions slowing down in the retarding field by the reducing distance between time markers. See text for details.

field and that the overall trend of the retardation pulse would be observed.

In practice, pulsing up the potential of the "exit" endcap could also have served to retard the injected ions however, from injection simulations, it was observed that pulsing down the "entrance" endcap potential provided a much more effective retardation force. This was because of the shape of the field lines in each case. The "entrance" endcap retardation field lines had a focusing effect on the incoming ions which encouraged them to remain in the centre of the trap while the "exit" endcap retardation field lines had a defocusing effect which directed the beam away from the centre of the cavity, towards the wall of the ring electrode.

C) Extraction

After a certain storage period had elapsed the ions were extracted from the trap by switching the potential on the "exit" endcap. The extraction impulse drew the trapped ions out through the screened "exit" endcap aperture. The height and duration of the pulse was such that the combination of the two provided sufficient energy to the trapped particles so that they exited the cavity in one bunch. If insufficient energy was provided the ions were ejected as two peaks, staggered by one RF cycle, or the signal was simply attenuated. Typical extraction pulse amplitudes were of the order of 200 V for a 4.2 μs duration. The timing of the pulse was synchronised with the RF.

Figure 3.7 is a simulation of the effect of an extraction force on ions inside the trap cavity. In this calculation the ions started at rest on the plane A. They were subjected to an extraction force produced by defining the "exit" endcap electrode potential 200 V below that of the ring and "entrance" endcap. The extraction force drew the ions out the aperture in the endcap. From the diverging spacing of the time markers one observes that most these ions exit the trap in less than 2 us. Again this simulation is used only to demonstrate the general effect of the extraction pulse, there would be a phase dependent influence due to the RF field.

It would also be possible to extract the ions from the trap by switching up the potential on the "entrance" endcap and effectively pushing the ions out the "exit" endcap aperture. However,

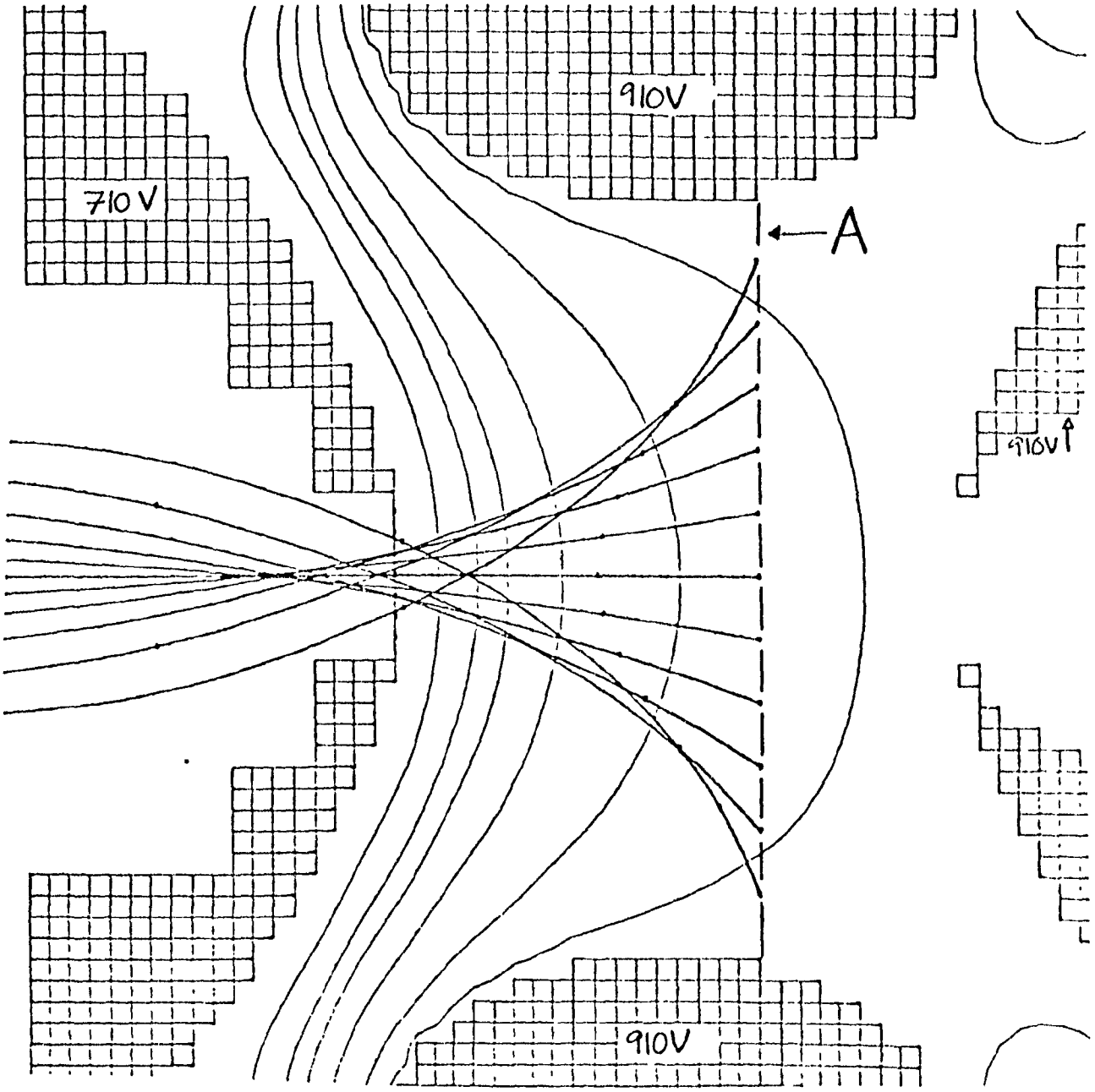

Figure 3.7: Simulation of ion motion inside the trap cavity under the influence of an extraction pulse. At t=0 the ions are at rest and located on the plane A. The dots on the ion trajectories are time markers, their spacing is 1 us. Observe the focussing of the ion cloud through the "exit" endcap aperture and the subsequent colimation of the beam.

from simulations the "exit" endcap was shown to be much more effective than the "entrance" endcap for this function. "Entrance" endcap extraction had a defocusing effect that spread the trapped cloud towards the walls of the cavity while the "exit" endcap method focused the cloud out the aperture as shown in figure 3.7.

3.4) Ion Detection and Data Acquisition

Upon leaving the trap cavity ions passed through a grounded screen located approximately 1cm from the "exit" endcap. Another positive effect of "exit" endcap extraction can be observed from figure 3.7. The natural collimation of the beam upon leaving the trap directed the ions along the axis of the flight tube towards the detector. A second einzel lens E2, 15cm from the screen, was used to focus the beam onto the multichannel plate detector D2 located at the end of the drift tube another 30 cm away.

Ions were detected by means of two multichannel plate (MCP) detectors, D1 and D2. Each detector consisted of two MCPs and suitable electronics were used to maintain appropriate biassing levels across the plates. One detector (D1) was mounted on a sliding rod and could be lowered to a position 15 cm from the "entrance" endcap on the beam axis. It was used to monitor ion production and transport prior to injection into the trap. When not in use it was retracted from the flight path and kept at ground potential. A second detector (D2) was placed on the opposite side of the trap at the far end of the extraction drift region. It was used to monitor the trapping and transmition of ions from the trap to the detector, (see figure 3.1).

Prior to the final assembly of the apparatus a calibration between the two detectors was made. The detectors were placed in series, 5 cm apart with D1 in front. A PLIS was directed towards them. Spectra from each detector were alternately recorded by raising or lowering D1 into the beam path. The integrated spectra from each detector were compared to determine the relative area a similar signal covered on each. The integration of the spectra was approximated

by the sum the channels in mV multiplied by the bin width in us. Thus, in the final assembly of the apparatus the relative number of ions observed in individual mass peaks could be determined. Comparisons of the signal area at detectors D1 and D2 were used to determine the efficiency of the system.

The output of the each of the two MCP detectors was viewed on a 100 MHz Hewlett Packard digital oscilloscope. Because of shot-to-shot variation of the source each spectrum was averaged over 16 shots before it was recorded. A digital readout of the spectra was transferred to an IBM XT PC and later to a PS/2 386 for plotting and analysis.

3.5) Electronics and Experimental Control

A) Timing

The experiment began with the production of an ion pulse. The ions were accelerated towards the trap and each mass group arrived at a different time, differentiated by their masses. A second trigger was required to initiate the retardation of one of the q/m ion clouds. The timing of the retardation pulse with respect to the source production was determined empirically by monitoring the transmitted signal on the detector D2 while adjusting the pulse delay. When the retarding pulse was appropriately timed a marked reduction in the number of ions, particular to that q/m group, transmitted through the trap could be observed. A typical firing-retardation delay was on the order of 10 us. A third trigger was required to initiate the extraction of the ions from the trap. For most of the results presented here the ions were trapped for 150 μs before extraction unless otherwise specified. See figure 3.8 for a schematic of the timing and triggering system

A variable frequency pulse generator supplied the master trigger, all subsequent triggers were derived from it. Work was generally conducted at a rate of about 2 Hz. This signal was synchronised with the RF phase and sent to an ORTEC model 416 Gate and Delay Generator

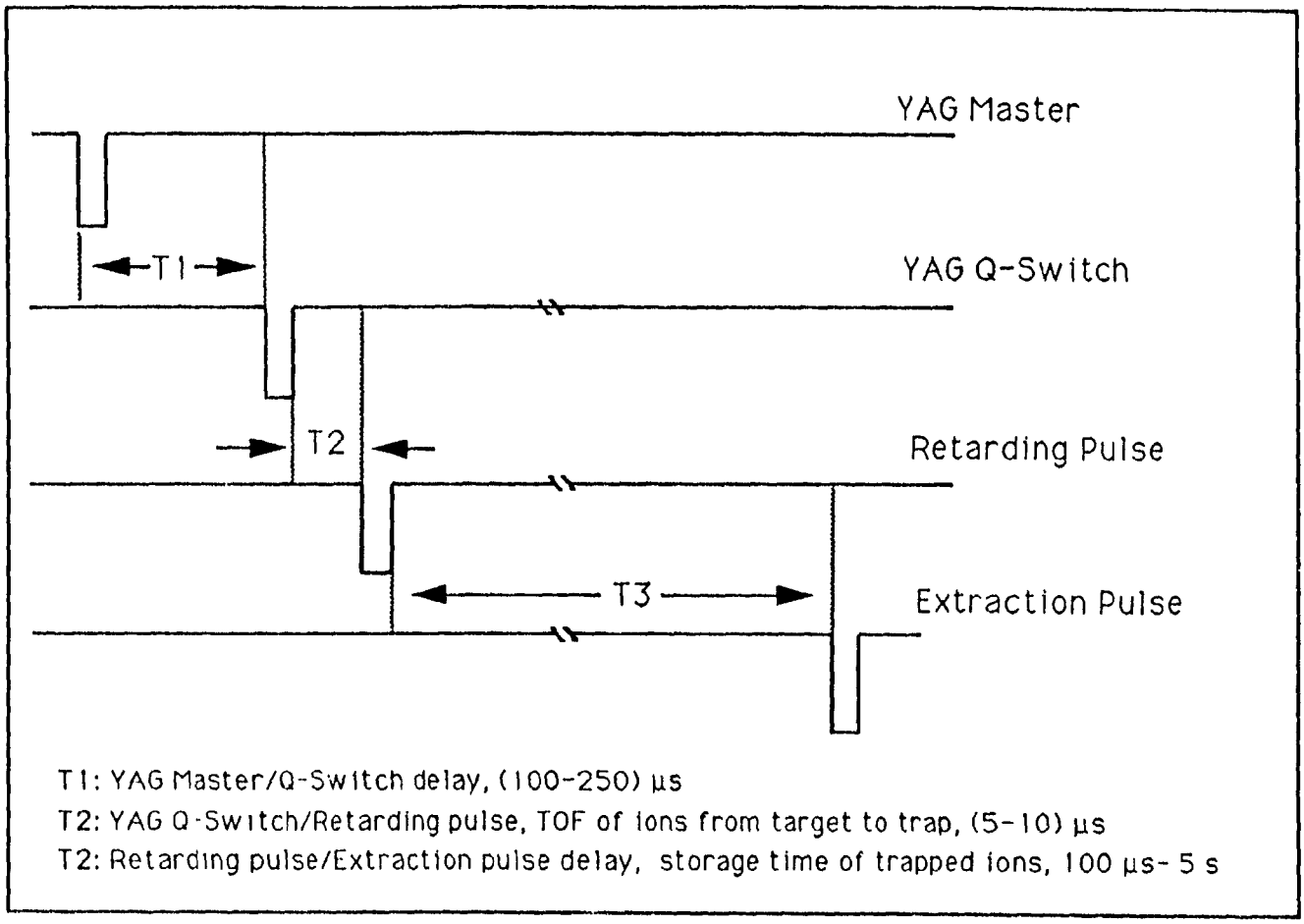

Figure 3.8: Triggering Scheme

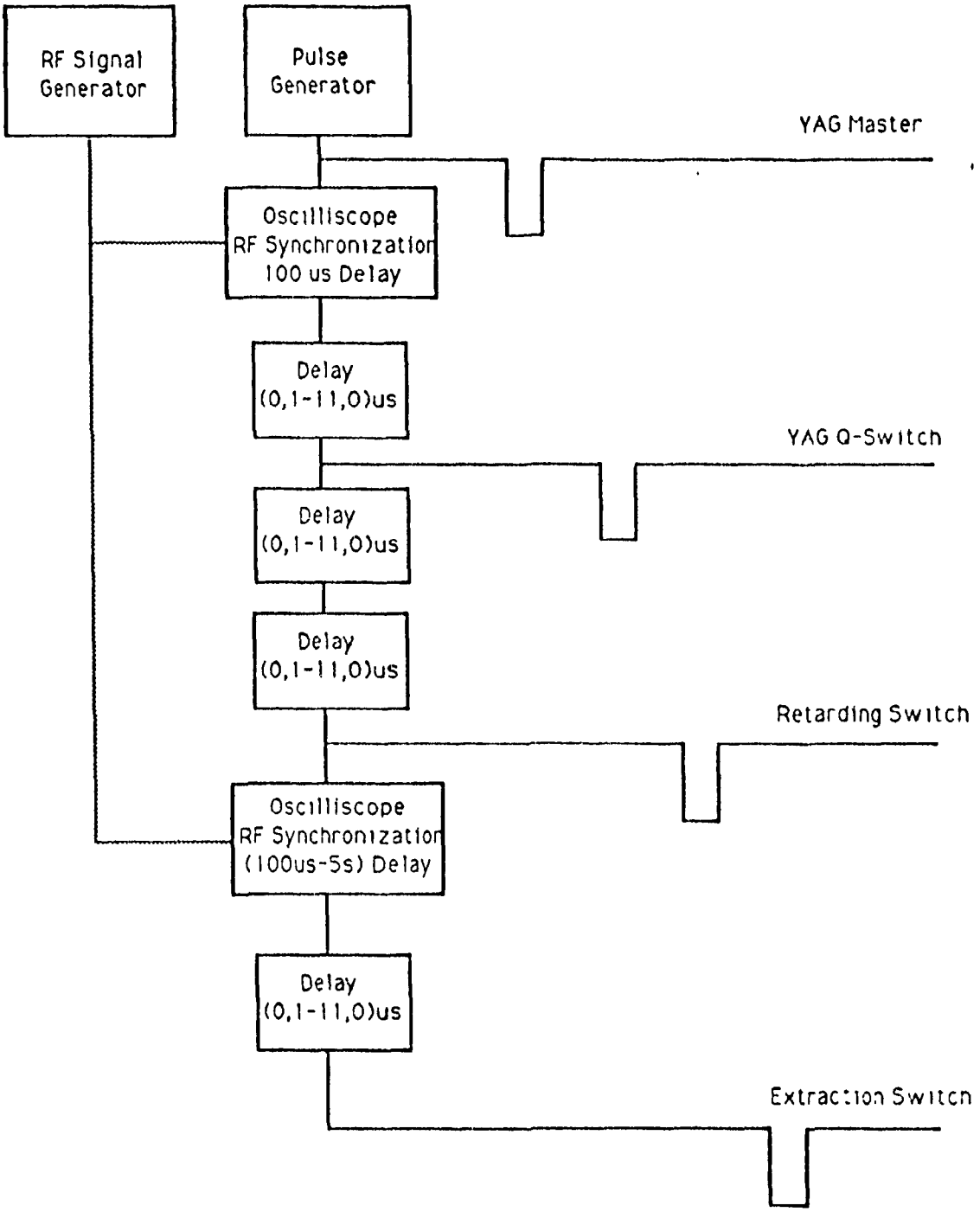

Figure 3.9: Timing Electronics

for fine tuning and RF phase variation before triggering the laser firing. The firing time could be varied on a 0.01 - 11.0 μs scale with respect to the synchronised RF phase. The retardation pulse was delayed from the laser firing on a similar ORTEC model 416 delay gate. (See figure 3.9)

The extraction pulse had two-step delay system. The firing trigger was first delayed on a large scale (up to 5 secs) and synchronised with the RF phase. This synchronised delay was obtained from the B trigger + delay feature of a Tektronix model 465 oscilloscope. It was then sent to an ORTEC model 416A delay gate for fine tuning on a 0.01-11.0 μs scale. The advantage to such a two-step delay system is that the trapping time can be varied over a large scale while the fine tuning of the extraction timing with respect to the RF phase remains constant.

B) Power Supplies and Switching

The target holder was held at a 1 KV potential provided by a FLUKE model 412A supply. The power supply for the accelerating plate, both einzel lens E1 and E2 and the injection lens was provided by an ORTEC model 210 supply.

The HP Harrisson model 6516A provided all the various DC levels to the trap electrodes by means of a divider circuit, (see figure 3.10). (Unless specified DC potentials are given for trapping positive ions. Signs are reversed for experiments trapping negative ions.) All three electrodes were maintained at an average base floating voltage of 910V. By means of a high voltage (HVSW1 on diagram) switch the "entrance" endcap could be pulsed as low as 75% of the base floating voltage to provide the retardation pulse. This same but independent feature on the "exit" endcap supplies the extraction pulse, (HVSW2).

An additional RF potential in the range of (200 V - 400 V) was applied to the ring electrode. The RF potential was obtained from a Tektronix model 190A signal generator. It was then amplified by a EIN model 325 RF power amplifier and finally by a 20X wire wound transformer bfore being applied to the ring.

he detectors, D1 and D2, were not used in tandem and the power was supplied to each alternately by a FLUKE model 412A power supply.

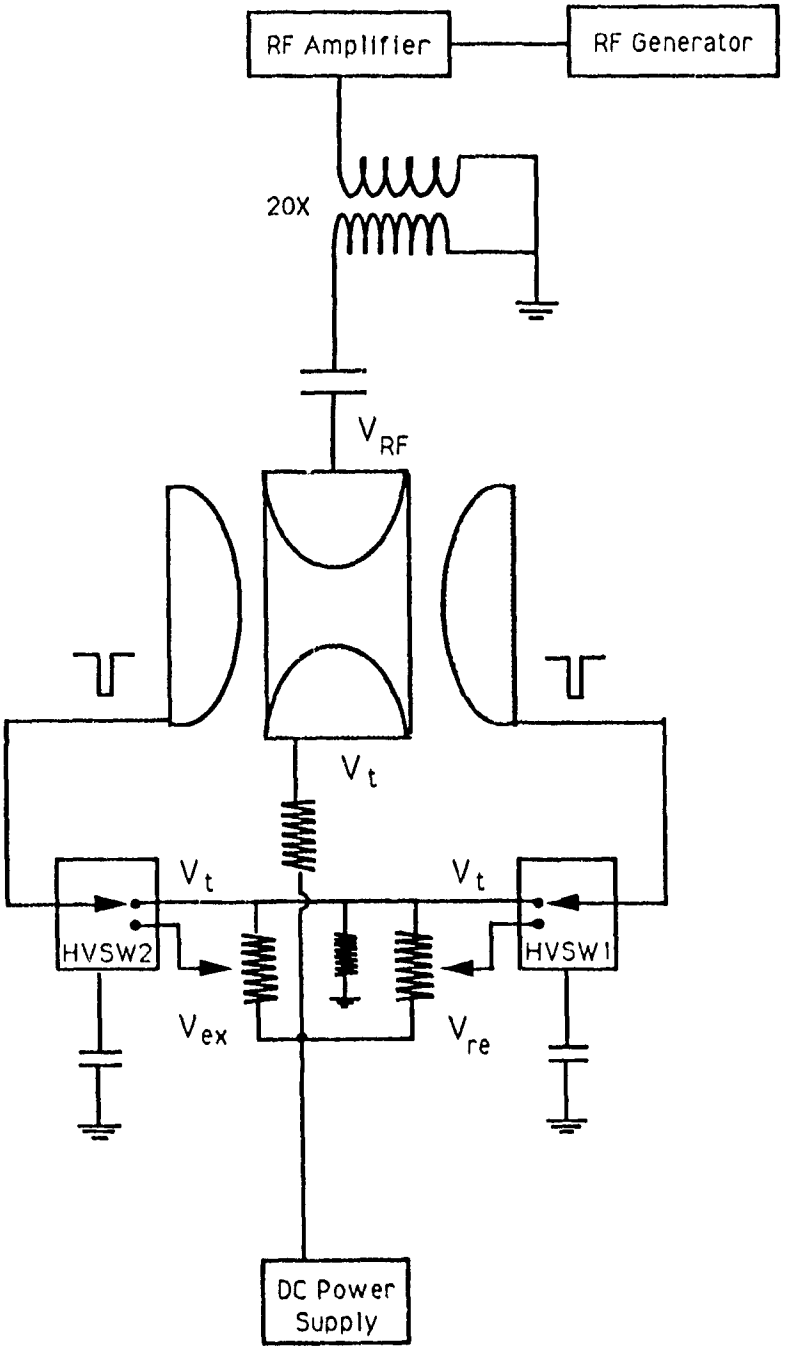

Figure 3.10: Switching Circuit

Chapter IV

Results and Discussion

4.1 Introduction

The capture and storage of ions required precise tuning of several parameters. These included the timing of ion production, the transport, focusing and deceleration of the injected ion beam, the timing of the retarding pulse as well as its strength and duration. The RF potential frequency and amplitude of the trap had to be tuned to establish a stable holding environment for any given mass and the extraction pulse strength, duration and timing were also subject to adjustment. Improper tuning of any one of these parameters resulted in an inability to trap ions.

In order to understand the results presented later in this chapter, an example of a typical spectrum one would obtain in this work is introduced and discussed in section 4.2. Following that, the results from a series of experiments designed to establish the working conditions of the trap are presented. These include establishing the storage efficiency (decay time of captured sample) of the trap as well as the relationship of the RF phase of the trap and the extraction pulse with the corresponding extracted signal. The results from experiments particular to the injection of ions into the trap are then presented. These are the RF phase of injection and the strength and timing of the retarding pulse. The selective capture of ions from two different mass groups in source is demonstrated. Lastly the overall efficiency of the injection system is evaluated.

4.2 Trapping

Figure 4.1 is an example of a TOF spectrum taken at the far detector, D2. The signal from a photodiode indicating the arrival of the laser light at the graphite target marked the time zero and started the digitizing process of this TOF waveform. Ions were created at the target surface and accelerated towards the trap. The C_2^+ cloud reached the "entrance" endcap of the trap first, the C_3^+ cloud arrived approximately 3.5 μs later. The two peaks in the area of 15-20 μs are ions from the C_2^+ and C_3^+ groups respectively, transmitted through the RFQ trap cavity. A retarding pulse, as described in section 3.3b, was applied. These transmitted ions thus represent those that were not sufficiently retarded inside the trap and left the cavity through the "exit" endcap aperture.

The height of the transmitted C_2^+ mass peak is much reduced compared to the spectrum presented in figure 3.4, this is because the spectrum shown was obtained by adjusting the timing of the retarding pulse to capture ions from the C_2^+ group. The transmission of ions from this group is likely due to the spatial distribution of the injected ion bunch, not all the ions in the group could be sufficiently affected by the retarding pulse. Since the timing of the retarding pulse did not correspond to the arrival of the C_3^+ peak at the trap, they were not subjected the retarding impulse inside the cavity and hence were all either transmitted or lost to the trap electrodes.

The captured C_2^+ ions were stored for 150 μs before the extraction pulse was applied. These ions were pulled from the trap and after drifting to the detector (D2) the extracted ion peak was recorded. This group of extracted C_2^+ ions can be seen at approximately 165 μs on the spectrum, corresponding to the storage time and the TOF of the ions from the target to the detector D2. Should any C_3^+ ions have been trapped their mass peak should have appeared at a later time. TOF considerations confirmed that the mass of the extracted ions corresponded to that of the C_2^+ cluster.

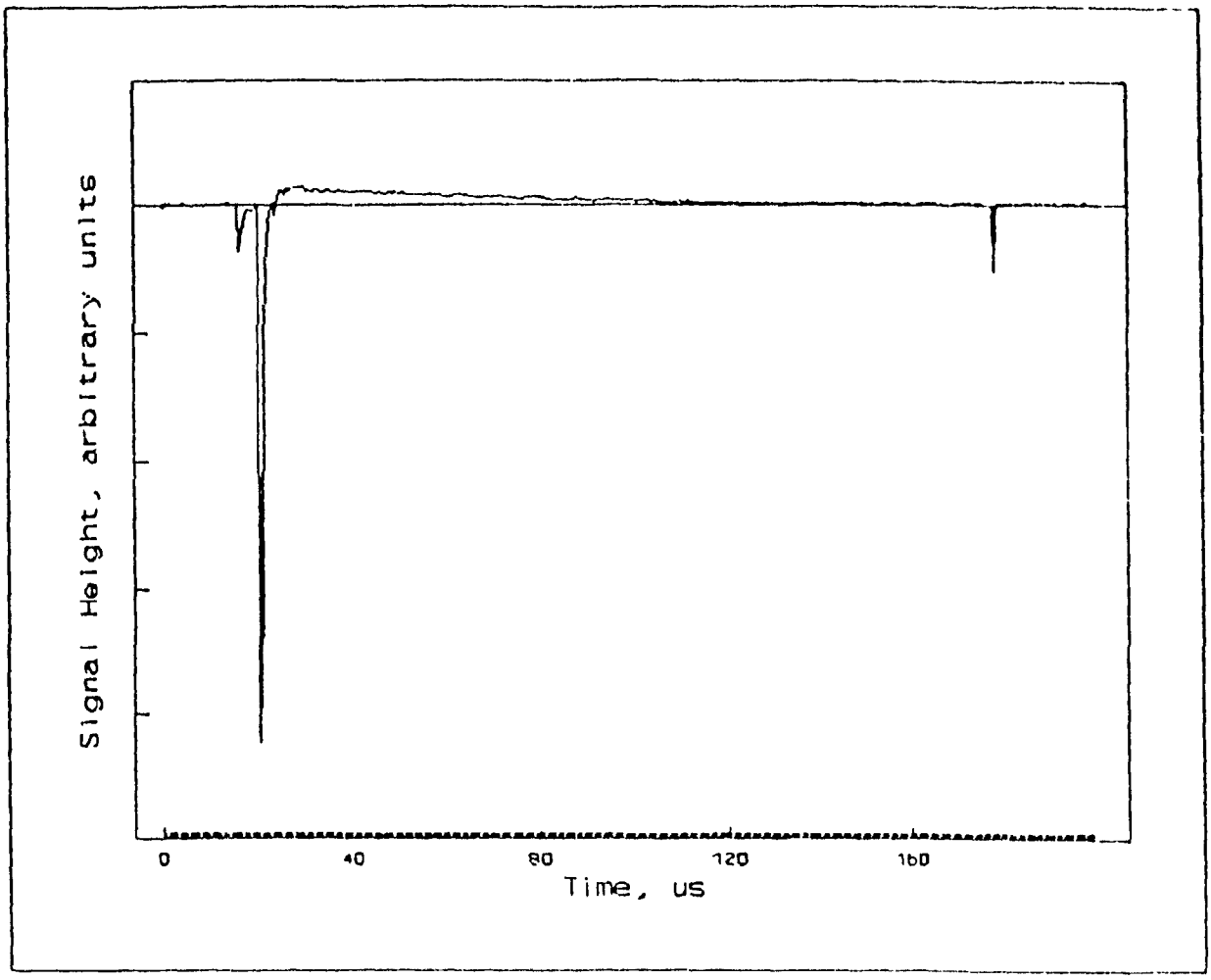

Figure 4.1: Typical TOF spectrum of including transmitted and trapped ions, taken at detector D2. Time zero is defined by arrival of laser light at the target.

4.3) Phase Dependence of Extraction

The effect of varying the RF phase of the extraction pulse was investigated. To do this the extraction pulse delay was varied in increments of 0.1 μs with respect to the RF phase of the trap while monitoring the extracted ion signal. The shape of the signal was observed to change with the phase of extraction. Figure 4.2 plots the extracted signal height against the relative delay of the pulse over several RF cycles. The height of the signal was measured using the digital voltage markers on the HP oscilloscope. The associated error on these measurements was approximated by recording a signal and repeating the measurement several times. The standard deviation was less than 3% of the measured signal height.

From the figure a phase relation to the shape of the extracted peak can be observed. The subtleties of the shape fluctuation did not digitize well due to the slow sampling speed of the oscilloscope and were further blurred in the averaging. Individual spectra could not be compared because of the shot-to-shot variation in ion production. A sketch of the sequence of the signal variation over RF phase is presented in figure 4.3. It demonstrates the shape variation of the extracted signal over half a cycle. The shape of the peak would change from (a) to (e) and back again over one full RF period. A second dependence on the β_z oscillations of the ions inside the trap could also affect the extracted peak size. However, this dependence was only obvious at β_z frequencies which were integral numbers of the RF frequency. Since this was not the case, given the parameters used for these experiments, variations due to this factor were not significant enough to be observed.

The fluctuation of the shape of the extracted peak with the RF phase is a well studied phenomenon and is explained by the variation of the phase space volume of the ion cloud inside the trap as a function of the RF phase (LU92). For this work, which was principally to investigate the injection phenomena, it was sufficient to note that the extraction phase must be maintained to resolve the TOF of the extracted peak and that some variation in the size of the signal could be seen at different extraction phases.

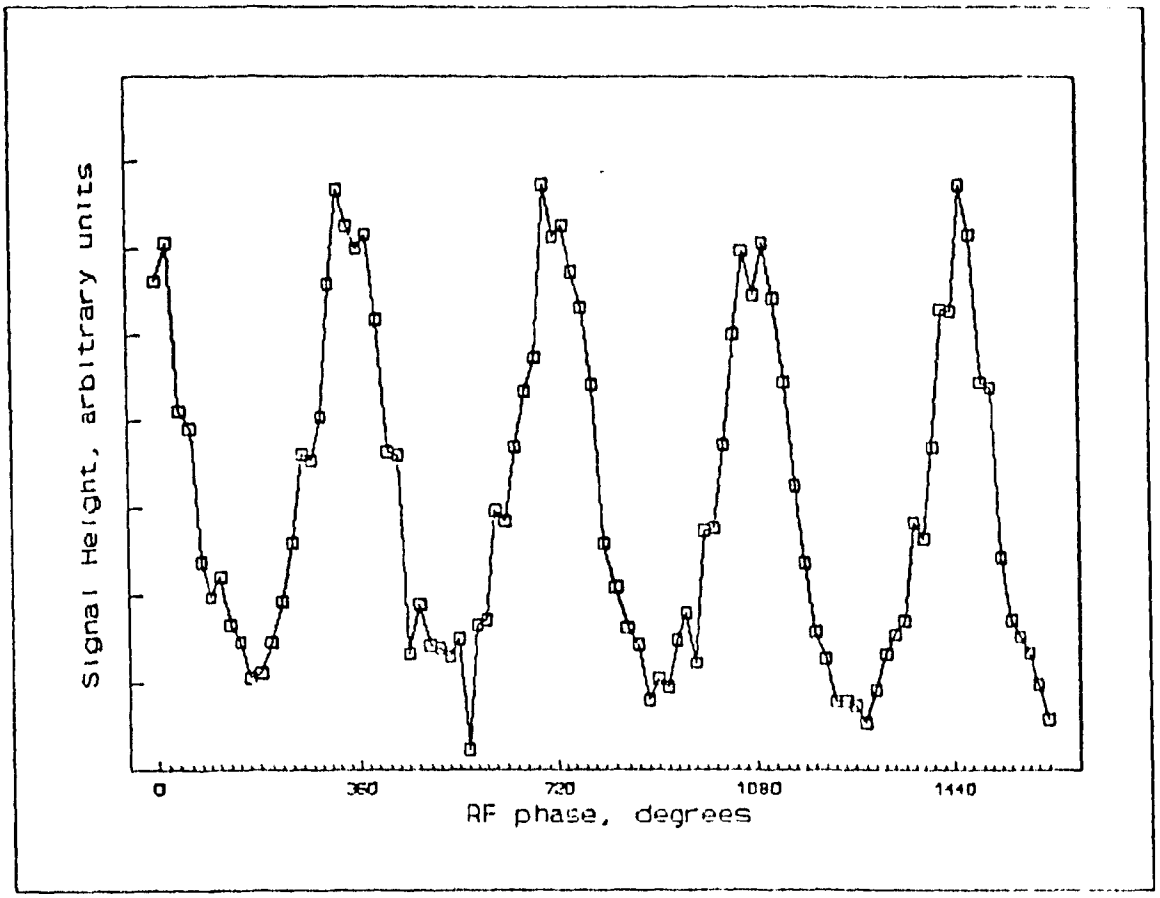

Figure 4.2: Signal Height Variation with RF phase of Extraction.

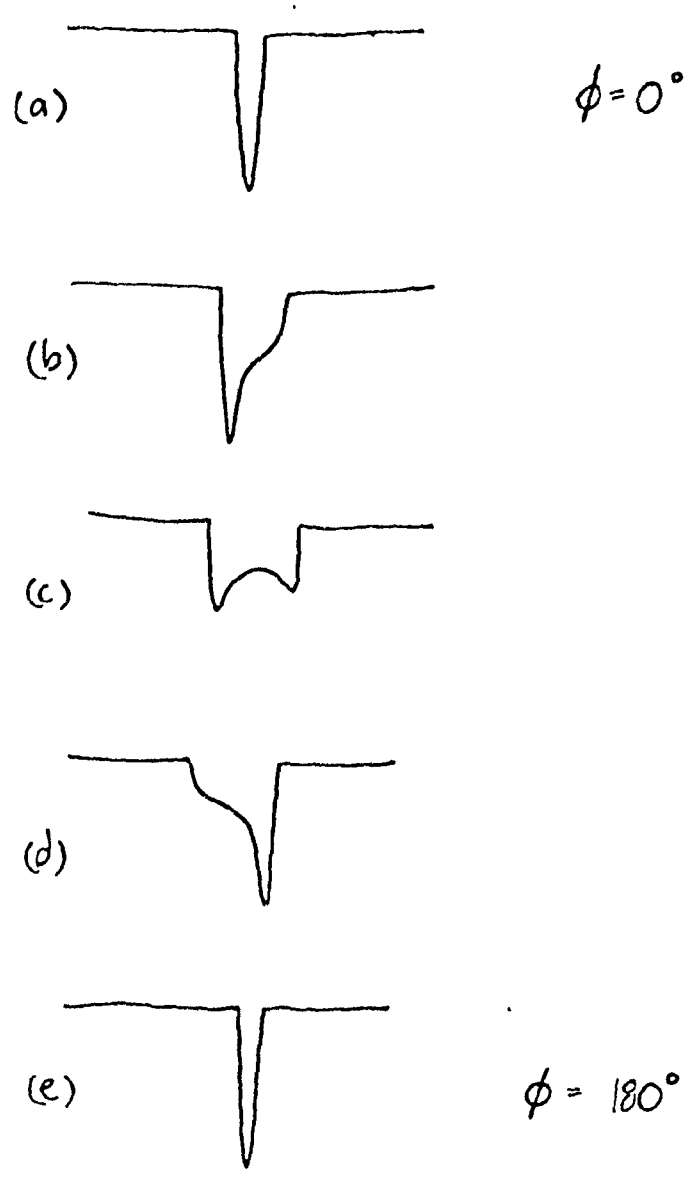

Figure 4.3: Sketch of extracted peak shape variation as extraction pulse timing is varied over one RF cycle.

4.4) Trap Storage Efficiency

The trap storage efficiency was evaluated by monitoring the extracted signal size over increased trapping periods. The holding time was extended by delaying the extraction trigger while keeping its phase constant with respect to the RF cycle. Figure 4.4 is a plot of the extracted signal size for a trapping periods ranging from 50ms to 1s. The signal size is plotted on a log scale.

Loses are primarily due to destabalising collisions between ions or with with residual gas particles inside the vacuum. One would expect the decay trend to be exponential if this were the sole reason for losses. Though the curve is roughly exponential for long holding times, it appears to flatten out for shorter ones. It is believed that there were two similar yet distinct phenomena accounting for this trend.

The equations introduced in Chapter II to describe the stability of an ion in an RFQ trap were derived for the case of a pure quadrupole field, however in practice there may be sevecal higher order components present due to the finite size of the trap or abberations on the electrodes (BO90). The addition of higher order fields will cause a coupling of the r-z motion and in some cases a destabalising effect on the trapped ions. The "leakiness" of the traps field refers to the presence of non-quadrupole components inside the trap. It is likely that the RFQ trap employed for these experiments had physical imperfections and non-quadrupole components to the electric field were present.

An example of the effects of higher multipole components on the ion motion inside the trap have been calculated by J. Frazen (FR91). Figure 4.5 taken from (FR91) is a simulation of the effect of superimposing a 2% hexapole component onto the quadrupole field on the ion trajectory in the axial direction for two sets of initial conditions. Observe the reasonant growth of the ion trajectory until it eventually collides with the endcap electrode at z_o. Because of the nature of the restoring forces, ions in the periphery of the trap cavity possess greater amounts of kinetic energy than ions near the center. They are therefore less stable inside the trap and more likely to leave or collide with one of the electrodes.

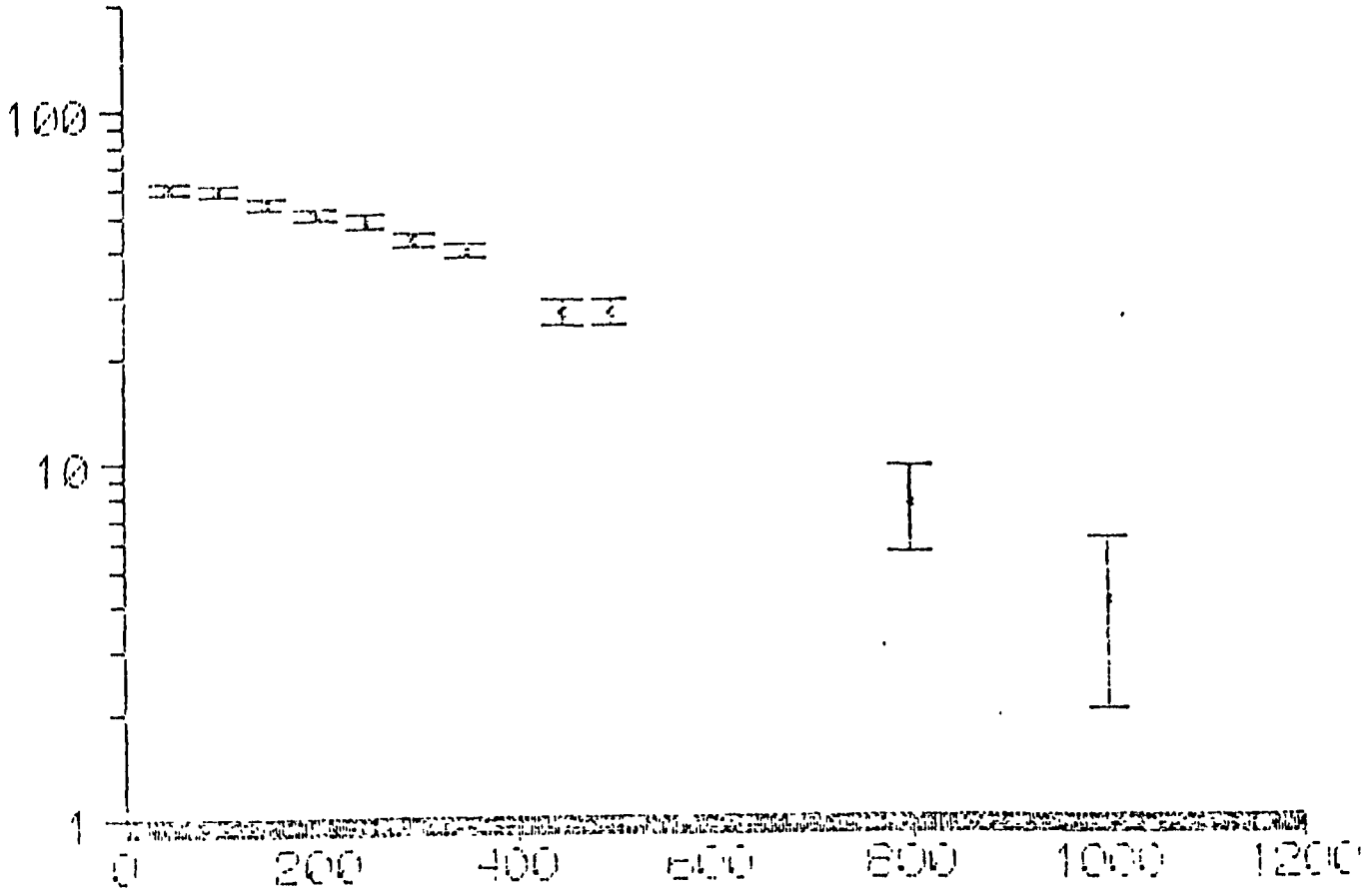

FIGURE 4.4: Semi-log Plot of Signal Size vs, Holding Time. The signal size is plotted on the the y-axis which is a log scale and the units are arbitrary. The x-axis represents the holding time, the units are in ms.

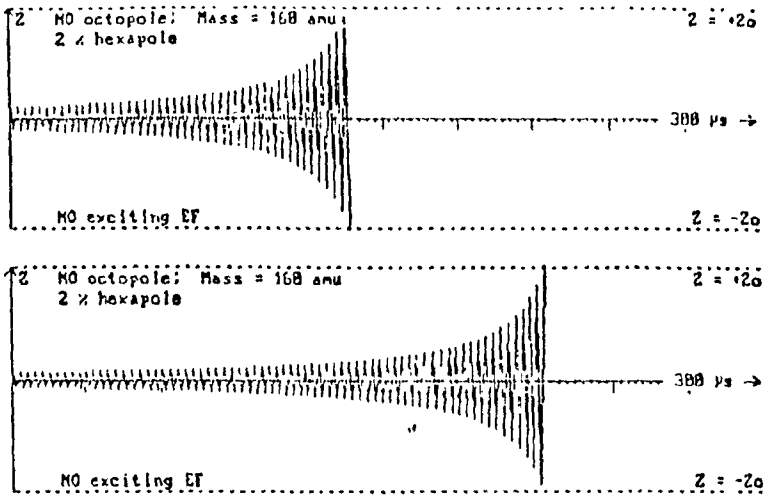

Figure 4.5: Simulation of the effect of a 2% hexapole component superimposed onto the quadrupole on the trajectory of a trapped ion along the z-axis. Taken from (FR91).

A second effect only observed for shorter holding periods may be responsible for the non-exponential decay at shorter trapping times. Injected ions that were stable in the trap still possessed varying levels of residual kinetic energy. Ions with less residual kinetic energy remained near the center of the trap and were the most stable while trapped ions with more kinetic energy occupied larger orbitals. The extraction and transportation of these ions with their greater amounts of kinetic energy, distributed in random directions, to the detector would not have been very efficient. The signal at D2 would not have represented the actual trapped yield since many of the extracted ions could have been lost before reaching the detector. Since these ions were already less stable than those near the center they would be the first to be lost in a "leaky" trap and this effect would not have been observed at longer trapping times. Therefore the yield for shorter holding periods would have appeared smaller than it actually was.

Thus it is believed that there may have been up to three seperate phenomena accounting for the observed decay trend of the trapping yield: destabalising collisions with residual gas particles, higher order fields and the ion optics between the trap and the detector D2. All of these effects are the result of trapped ions possessing residual kinetic energy and could be reduced by cooling the ion cloud inside the trap. It has been shown by J. Yoda et al. (YO89) that the addition of a light buffer gas to cool the trapped ion cloud through collisions greatly improves the holding efficiency of the trap since cooled ions tend to the center of the cavity. Having established the effectiveness of the retarding mechanism, low levels of buffer gas could be introduced to cool the trapped ions through collisions to increase the holding efficiency.

4.5) The Retarding Pulse

The role of the retarding pulse was to reduce the kinetic energy of ions injected into the trap. Simulations using SIMION predicted that the retarding pulse would have a maximum effect if applied just as the injected ions entered the trap cavity. Figure 4.6 demonstrates the effects of varying the time at which the retardation impulse was applied relative to the source production. Since the time of flight of the ions remained constant, this constituted varying the retarding pulse

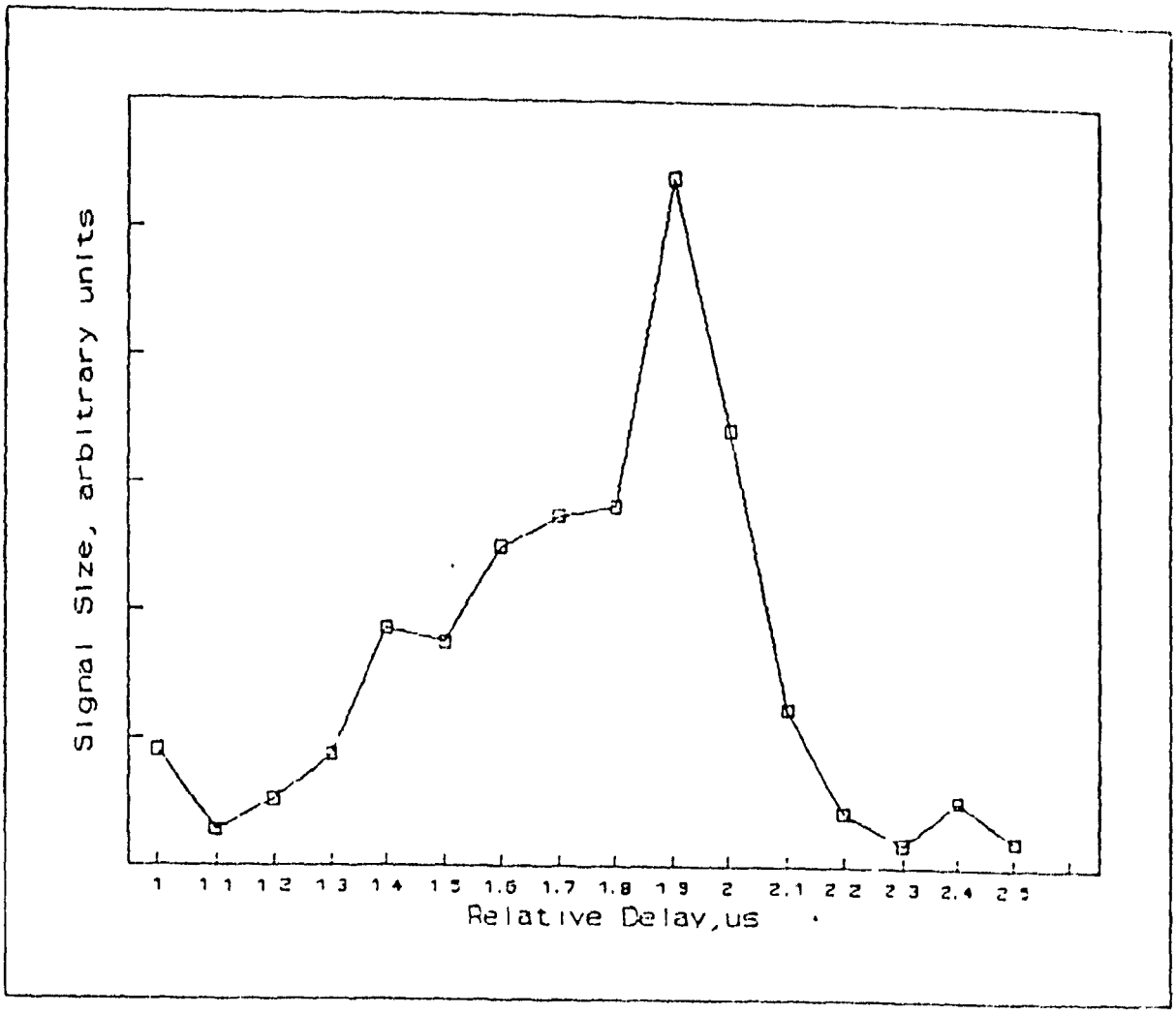

Figure 4.6: Variation of trapped signal size w r t. delay between the arrival of ions at the trap and the application of the retarding pulse.

with the physical position of the ion cloud with respect to the "entrance" endcap. The relationship between the number of ions that remained trapped for 150 μs and the time at which the retardation pulse was applied indicates a maximum, which can be seen at 7.6 μs for the C_2^+ peak.

The effect of varying the strength of the retarding pulse was also investigated. The maximum yield corresponded to a pulse with an amplitude of 165 V and a 660 ns width. The height of the pulse was gradually reduced in increments 10-15 V until it reached 115 V which marked the threshold for trapping. Results for four different retarding voltages are presented in figure (4.7) which plots the ion yield vs. the pulse timing for each of the four different amplitudes.

From these results the following simple model was proposed for calculating the pseudo-potential well depth of the trap. The impulse from each of the pulses can be obtained from equation (2.31). From equation (2.32) it was shown that the effect of the retarding impulse could be evaluated if the gradient of the electric potential in the trap cavity could be established. Again considering that the influences of the RF field are oscillatory and result in no absolute energy loss to the ions, the following analysis was made.

Figure 4.8 is a plot of the electric potential field lines due to a 165 V potential difference between the "entrance" endcap and the other two trap electrodes. The trajectory for a 90 eV ion moving in the axial direction starting from point A is also included. At point B, slightly more than 1 μs later, the ion's kinetic energy was reduced to zero and it was accelerated out of the trap back along the same line. From this simulation it was observed that the equipotential lines due to the retarding field are approximately evenly spaced along the z-axis over the first third of trap (the area from the "entrance" endcap moving towards the center.) indicating that the potential was essentially linear in this region. Furthermore it was observed from the time markers that under these conditions a 90 eV ion did not escape the linear field region in less than 660 ns, (the duration of the retarding pulse).

Under these conditions an approximation of the potential gradient along the z-axis was made by

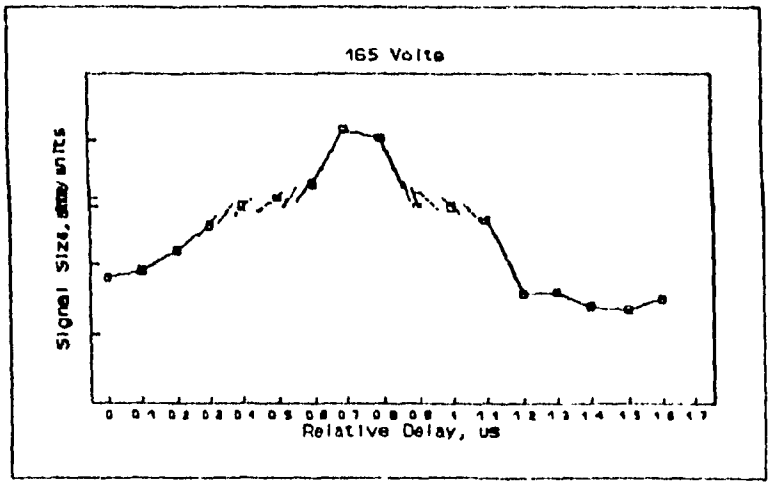

Figure 4.7a: Trapped signal size variation with a 165 V retardation pulse delayed in increments of 0.1 us w.r.t. the RF phase of the trap.

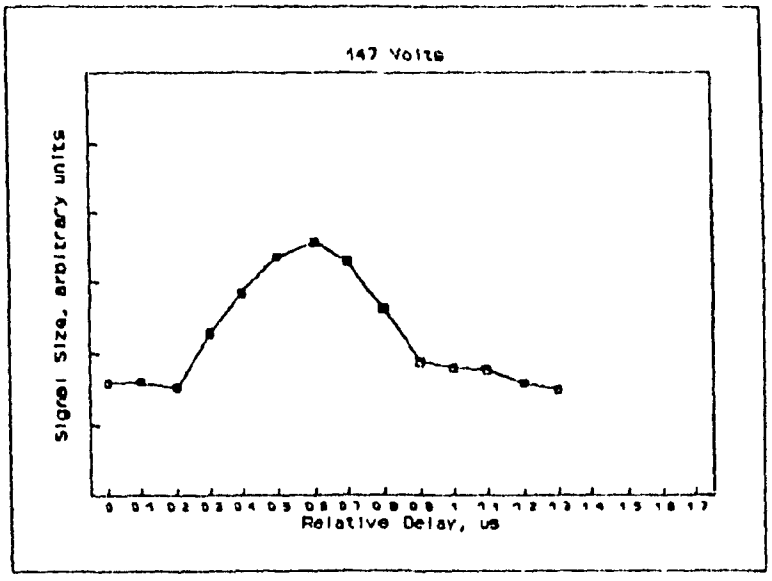

Figure 4.7b: Trapped signal size variation with a 147 V retardation pulse delayed in increments of 0.1 us w.r.t. the RF phase of the trap.

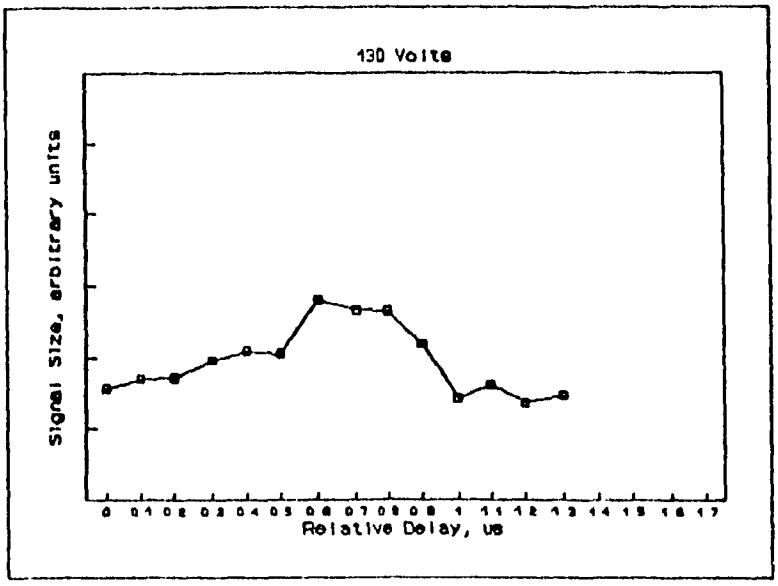

Figure 4.7c: Trapped signal size variation with a 130 Volt retardation pulse delayed in increments of 0.1 us w.r.t. the RF phase of the trap.

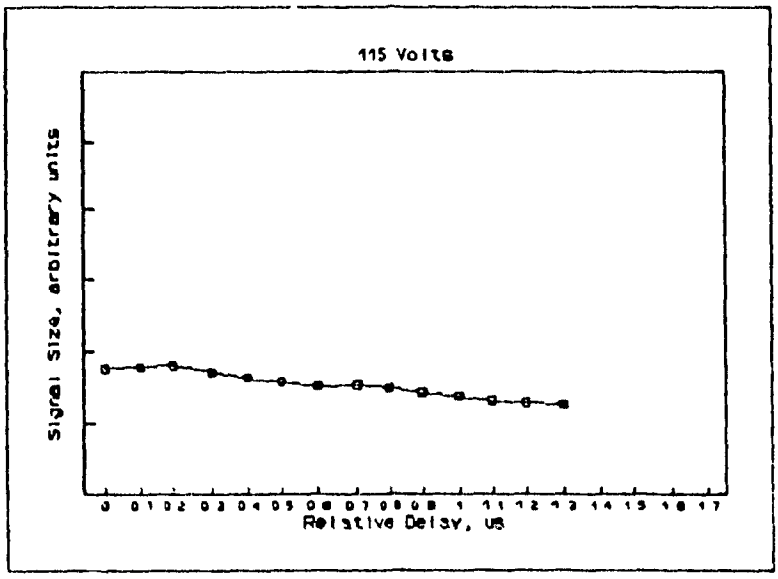

Figure 4.7d: Trapped signal size variation with a 115 Volt retardation pulse delayed in increments of 0.1 us w.r.t. the RF phase of the trap.

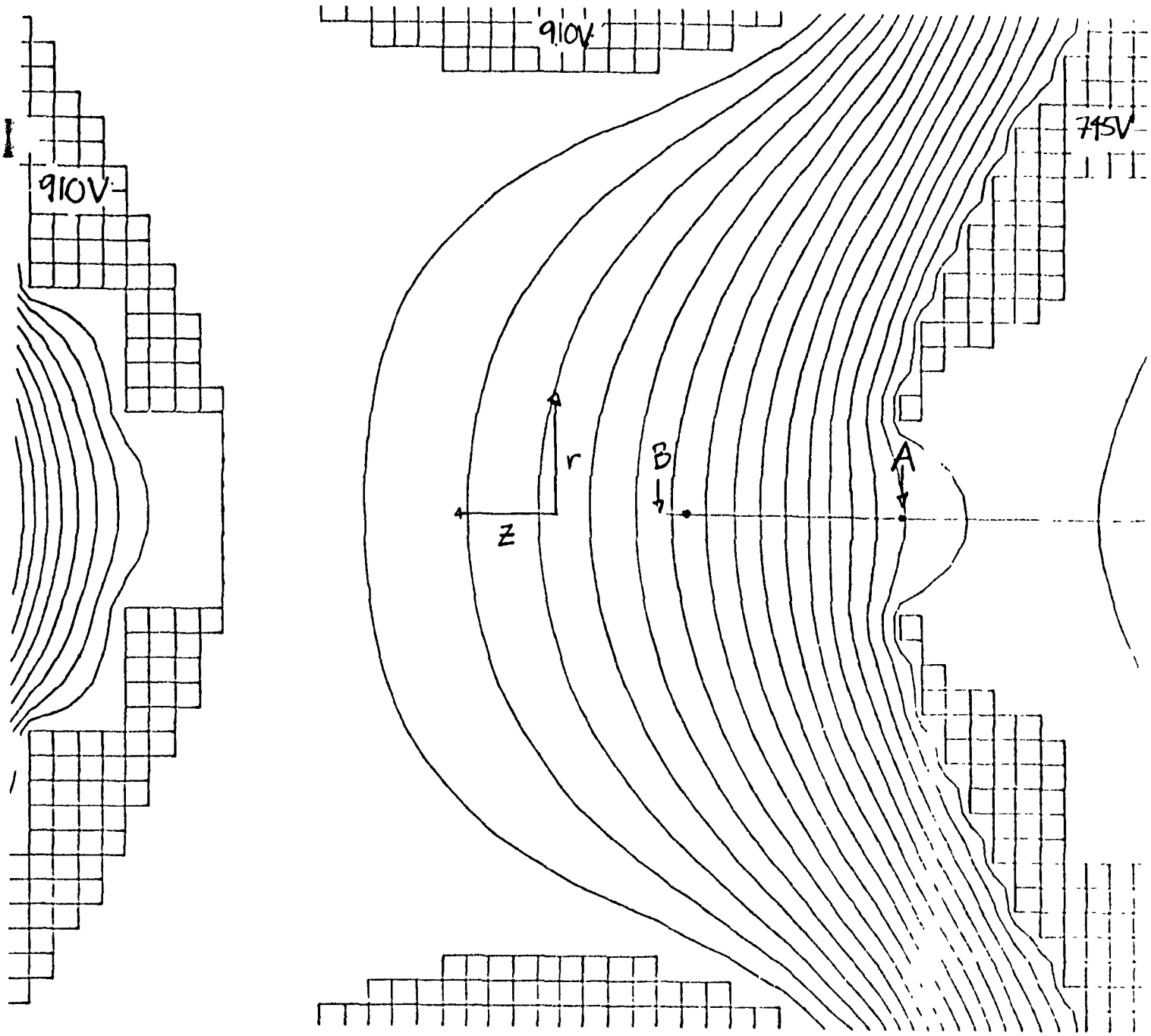

Figure 4.8: Equipotential lines due to a retardation pulse. An ion which starts at point A with 90 eV kinetic energy directed along the z-axis is retarded. It has zero kinetic energy at B and is accelerated out of the trap along the same line. The dots on the trajectory are 1 us time markers.

direct measurement from figure 4.8. The gradients for each of the other pulse heights were similarly obtained. The errors associated in making these approximations were estimated by comparing the potential differences between the broadest seperation of two equipotential lines and the smallest in the region in question. In this manner the estimated error increased as the pulse strength decreased since the ion then travelled further into the non-linear region of the trap during the 660 ns period of the pulse.

Using values for the potential gradient obtained in this manner and the equations (2.33) and (2.34) the residual kinetic energy of an ion with the initial conditions defined above, subjected to the various levels of retardation, were obtained. They are displayed in table 4.1.

Table 4.1: Effect of Retarding Impulse

Pulse Height, (V)	Energy Loss, (eV)	Final Energy, (eV)
165	74 ± 7	16 ± 7
147	58 ± 9	32 ± 9
130	44 ± 12	46 ± 12
115	32 ± 15	58 ± 15

From the table one observes that the residual kinetic energy of an ion subjected to a 165 V pulse was the minimum. Since it is known that the less energy the ions possess the more stable they are in the trap this explains the maximum trapping yield for this retardation potential. On the other hand the 115 V pulse, which marked the threshold retarding amplitude for trapping, left the ions with sufficient energy to escape the trap. This value represents the maximum kinetic energy an ion can possess and remain in the trap and the well depth of the trap can be estimated as 58 ± 15 eV. This was compared to the value for the pseudopotential well depth

obtained from table 3.1. For a mass 24 ion and the operating conditions of a 360 V, 650 Hz RF potential the axial-depth is 39 eV. The model is in reasonable agreement with the theoretical value, indicating the validity of the approach used in this work for retarding injected ions.

4.6) RF Phase Dependence of Injection

The phase dependence of the ion injection was investigated by varying the laser firing with respect to the RF phase of the trap. Since the drift time from the target to the "entrance" endcap and the relative timing of the retarding pulse remained constant this in turn varied the phase of the arrival of the ions at the "entrance" electrode. Figure 4.9 demonstrates the effects of varrying the laser firing with respect to the RF phase of the trap on the extracted ion yield. As was predicted a phase dependence between injection and trapping stability was observed. The width of the acceptence window was estimated by averaging the FWHM of the peaks. It was calculated as 90° ± 10°, this value was much larger than anticipated given the theoretical predictions.

Calculations of the RF phase acceptence angle for axial injection are on the order of 10° for 0-20 eV ions and expected to narrow for greater kinetic energies [(LU88), (081), (TO80)]. However existing models of the axial injection phenomena have only limited application to this work since none included an effective retarding mechanism. Only Lunney et al. (LU88) incorporated retardation into their model in the form of a small damping potential between the two endcaps to temporarily limit the axial displacement of the ions. Like the RF this retardation is oscillatory and does not retard the ions absolutely. It provides a temporary retardation of the injected ions which increases the amount of time they spend inside the trap cavity, and hence, the probability of their collision with the buffer gas to reduce their energy absolutely.

The trajectory of a trapped ion subject to collisional retardation would have been very difficult to calculate. Though it would appear to be reasonable to do so with an electrical retarding

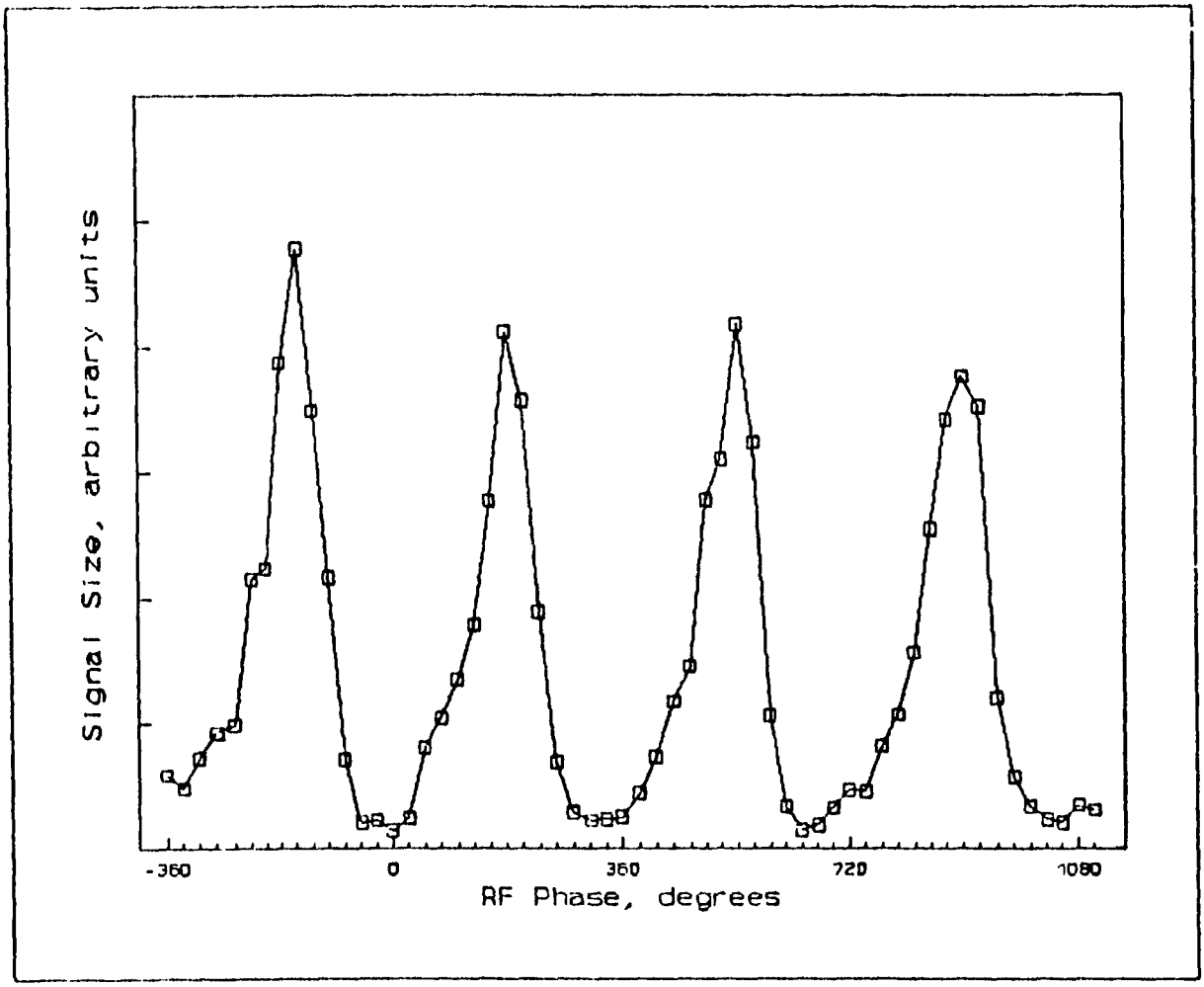

Figure 4.9: Variation of the trapped ion signal height as injection timing is delayed w.r.t. the RF phase of the trap.

potential, it has not been attempted. As a consequence the application of any of these models to the case of injection at hand, using a 90 eV ion subject to electrical retardation, is restricted. However, some comparisons can still be made and the following argument is offered as a possible explanation of the observations.

The relatively high energies of the injected ions (90 eV compared to values on the order of 20 eV used in theoretical calculations) in this work meant that they were able to overcome the RF field at the "entrance" endcap over a broader phase angle. Though they may not have been immediately accepted into stable orbits, a larger number were able to gain access to the trap cavity. Once inside they underwent a dramatic energy loss from the retarding pulse. The ions were then at a stage where they have accessed the trap cavity and reduced their kinetic energy. The retarding pulse had transformed the phase-space of the cloud which was otherwise unacceptable for placement into a stable orbits and brought it closer to the phase-space origin and the acceptance volume of the trap. At this point the problem became one of capturing from an internal source. Since a low energy ion cloud in the center of the trap is the most stable situation for confinement in an RFQ trap one would expect a broader acceptance for this case. Using this theory to explain the events, the success of the injection phenomena observed over the course of this work indicates that the energy and phase of injection are of lesser importance than the subsequent ion energy reduction for effective capture from an external source.

4.7)Mass Selective Capture

It was demonstrated that trapping individual q/m groups from the same source was possible by varying the timing of the retardation pulse. Figure 4.10a is a spectrum of the transmitted source in the absence of any retardation. The peaks correspond to the C_2^+ and C_3^+ clouds. They were slightly distorted by the RF field while passing through the trap. In the absence of a retarding pulse no ions were captured as was revealed by the lack of an extracted peak after the extraction pulse was applied at 80 us.

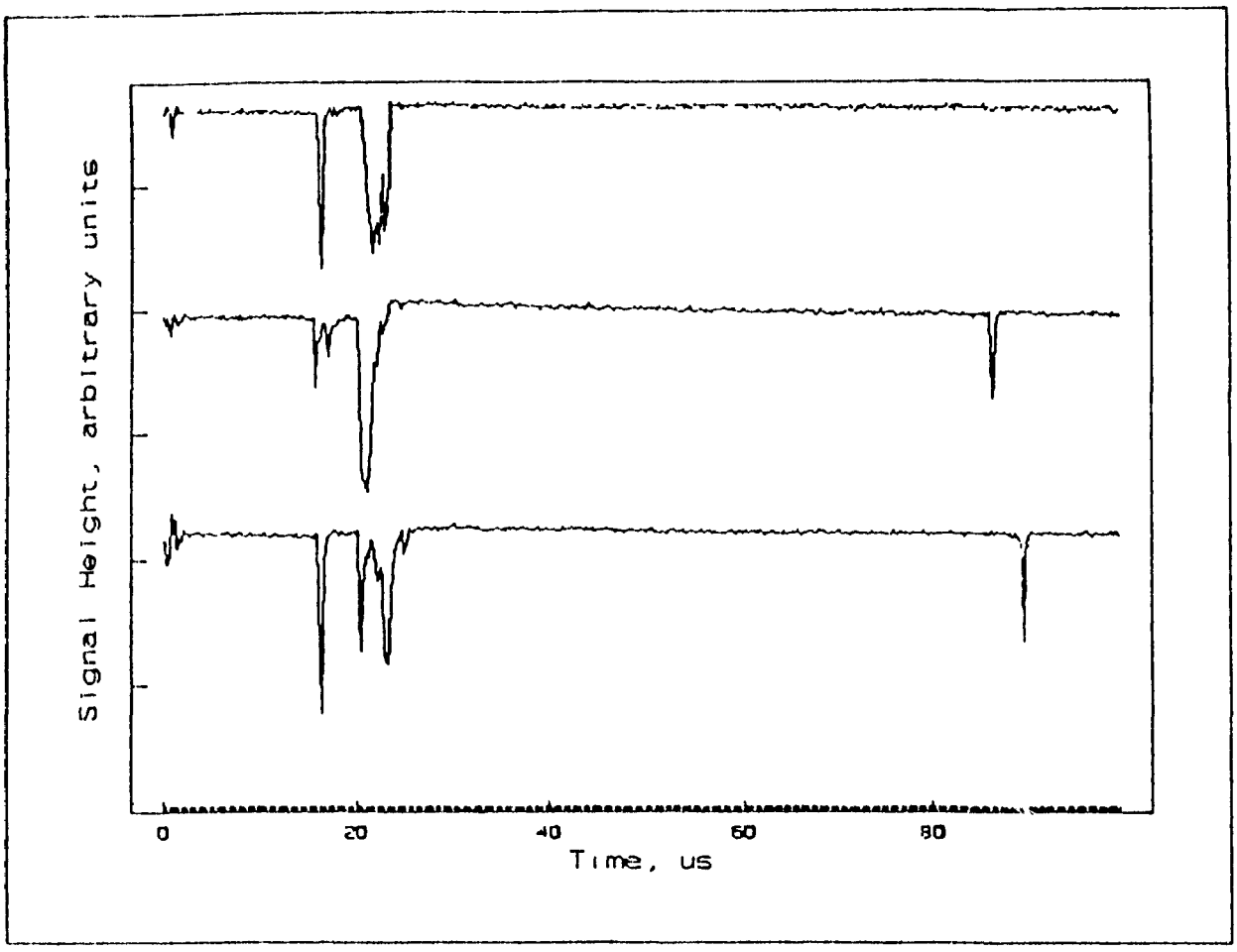

Figure 4.10: Three TOF spectra corresponding to different delays between source production and the application of the retarding pulse.

(a) No retarding pulse

(b) Production-retarding delay of 7.6 us

(c) Production-retarding delay of 11.0 us

The distortions of RF field aside this otherwise typical TOF spectrum indicates that the C_2^+ and C_3^+ ions are travelling at different speeds and will pass through the trap cavity at different times. Thus by varying the timing of the retardating pulse one could retard either of the q/m clouds inside the trap.

In figure 4.10b the retardation pulse was applied 7.6 μs after the ion creation. Observe that the transmitted C_2^+ peak was reduced while an extracted peak appears shortly after the extraction pulse was applied some 150 μs later. It is of interest to note that the retarding pulse appeared to have only affected the central portion of the ion peak. Also that the time base of the transmitted peaks appear to have broadened as a result of passing through the trap cavity. The C_2^+ peak base is now of the order of 2 μs wide as compared to 300 ns at detector D1. This will have consequences on the efficiency of the injection mechanism.

By increasing the retarding pulse delay to 11.0 us, ions from the C_3^+ group were captured as seen in figure 4.10c. The increased TOF of the heavier C_3^+ ions to the detector may be observed from the spectrum.

4.8) Trap Capture Efficiency.

The efficiency of the injection mechanism was estimated in the following manner. A spectrum of the ions transported from the source as far as the first channel plate D1 was recorded. The C_2^+ peak was isolated and its signal was integrated to estimate the total area and hence number of ions it represented. The detector D1 was then retracted and the retarding pulse applied to capture C_2^+ ions. These ions were trapped for 150 μs and the extracted peak was recorded on detector D2. The integrated spectrum of the extracted ion peak was compared to the spectrum taken at detector D1.

The results of repeated experiments varied, however using this definition, an efficiency between 3% and 6% was typical. Though this value compares quite favorably to estimations of 0.001 %

(LO89) and 0.02%[1] (MO92) overall efficiencies for continous beam/buffer gas cooling injection, one would expect that the overall efficiency of PLIS injection should be better still.

It is believed that the greatest limitations on this value were from two sources: the finite width of the injected mass peaks, and the ion optics. The base of the injected C_2^+ mass peak was evaluated as approximately 2.5 cm wide at the detector D1 in section 3.3b, this value is close to the 2.8 cm axial length of the trap cavity. Furthermore as was demonstrated in section 4.7 there is a broadening of the signal due to the RF near or inside the trap. Since the strength of the retarding field varied significantly over the entire length of the cavity (refer to figure (4.8)) it could not have effectively retarded the entire ion cloud. This effect was also seen in section 4.6 where the timing of the retarding pulse was varied and compared to the extracted signal size. Though a maximum in the size of signal was apparent it was also obvious that there was a broad, 1.5 us, time window over which ions were retarded sufficiently for capture due to the spatial diameter of the incoming cloud. Therefore one could assume that for any given run not all of the ions in the targeted mass group were effectively retarded by the 660 ns pulse. Also, the spatial width of the peak indicated a finite volume of the phase-space of the ion cloud and reduces the probability of acceptance of the entire cloud at any given RF phase.

The consequences of any of these factors would have reduced the effectiveness of the retarding pulse. The impact of this would have been observed as a reduction of the number of ions extracted to the number of ions injected and as a reduction in the overall efficency.

Losses of this nature could be reduced by decreas he patial width of the injected peak. Though some energy and spatial spreads are always inherent in the laser desorption process, to a certain extent they are correctable. It has been demonstrated by (MO90 and references therin) that a two-gradient sequential accelerating mechanism will reduce the energy and spatial spread of the pulsed source. The initial spatial distribution of the ion cloud could be further reduced by decreasing the size of the irradiating laser spot.

---

[1] 0.2% for 10% of the total beam

The effectiveness of the ion-optics in focussing the injected beam through the "entrance" endcap and transporting the ions from one area of the apparatus to the other also could have affected the evaluation of the capture efficiency. Since the spectra were each recorded at some distance from the "entrance" and "exit" endcaps of the trap, and it is believed ions were lost in transport. Thus, fewer ions were actually transmitted through the "entrance" endcap than were recorded at D1 and more ions were actually extracted from the trap than were recorded at D2. It is thus believed that this method of evaluating the capture efficiency may have resulted in an underestimation of the absolute injection efficiency.

One way of accounting for the loss due to the ion-optics is to examine the spectrum of a transmitted peak at detector D2. A transmitted peak of the C_2^+ ions is recorded without any retarding of the ions. This signal more accurately represented the number of ions that were actually injected into the trap and relative losses in transport would no longer affect the results since now both transmitted and trapped ion clouds travel the same path. Therefore, when compared to the extracted peak this method provides a more accurate gage of the injection/capture efficiency. Using this definition the efficiency of the injection mechanism is of the order of 25%. Though this figure makes some correction for the ion-optics it still reflects the losses due to the spatial width of the injected peak. It is predicted that an even higher efficiency could be achieved by controlling this factor.

Chapter V

Conclusions

An injection system was designed and tested to determine its feasibility for mass-selective capture of ions by an RFQ trap. Using this system, externally injected C_2^+ and C_3^+ ions were selectively captured from the same source. A capture efficiency of 25 % was attained indicating that a pulsed ion source coupled with an electrical retarding mechanism is well suited for effective capture by an RFQ trap.

The study of several of the system paramaters has helped to isolate the factors limiting the efficiency. It was determined that the most constraining influence was due to the spatial width of the injected ion pulse. Further studies on the broadening of the injected ion peak by the RF field of the trap can serve to determine whether bunching the injected ion cloud could improve on the capture efficiency of the system.

The FWHM for capture of injected C_2^+ ions was measured to be $90° \pm 10°$ of the RF cycle. It was determined that this value was particular to the phase space volume of the injected ion cloud and thus, could not be compared to the results of calculations found in the literature.

The effectiveness of an electric retarding potential in reducing the kinetic energy of injected ions for capture by the RFQ trap was evaluated. Based on these results a simple model to estimate the pseudo-potential well depth of the trap was formulated. Due to the simplicity with which the retarding pulse could be modeled, and its demonstrated success, it is proposed to be applied to existing theoretical models so that higher energy ion injection could be evaluated analytically.

(GO91) D.E. Goeringer, W.B. Whitten, Z.M. Ramsey, , Vol. 106, 175.

(HE89) D.N. Heller, I. Lys, R.J. Cotter, Analytical Chemistry, Vol. 61, 1083.

(JU87) K. Jungmann, J. Hoffnagle, R.G. Devoe, R.G. Brewer, Physical Review, Vol. 36, 7, 3451.

(KW89) V.H.S. Kwong, Physical Review, Vol. 39, 9, 4451.

(KW90) V.H.S. Kwong, T.T. Gibbons, Z. Fang, J. Jiang, H. Knocke, Y. Jiang, B. Ruger, S. Huang, F. Braganz, W. Clark, Review of Scientific Instruments, Vol. 61, 7, 1931.

(LU86) M.D.N. Lunney, MSc. Eng Thesis, McGill, 1986, unpublished

(LU89) M.D.N. Lunney, J.P. Webb, R.B. Moore, Journal of Applied Physics, Vol. 65, 8.

(LU92) M.D.N.Lunney, F. Buchinger, R.B. Moore , Journal of Modern Optics, Vol. 39, no. 2,349-360.

(MC78) M.D. McGuire, R. Petsch, G. Werth, Physics Review A, 17, 1999 (1978).

(MO88) R.B. Moore, S. Gulick, Physica Scripta, Vol. T22, 28.

(MO89) R.B. Moore, Transcript of talk presented at GSI, 1989.

(MO90) R.B. Moore, G. Bollen, "Electromagnetic Trap Particle Dynamics", unpublished manuscript, 1990.

(MO91) K.L. Morand, S.R. Horning, R.G. Cooks, International Journal of Mass Spectrometry and Ion Processes, Vol. 105, 13.

(NA89) M. Nantel, MSc. Thesis, McGill University, unpublished, 1989.

(O81) C.H. O, H.A. Schuessler, Journal of Applied Physics, Vol. 52, no. 3

(PA56) W. Paul and H. Steinwedel, Ger. Patent 944 900, (1956)

(SE88) G. Seifert, S. Becker, H.J. Dietze, International Journal of Mass Spectrometry and Ion Processes, Vol. 84, 121.

(TH90) R.C. Thompson, Measurement-Science Technology, 1, 93.

(TO80) J.F.J. Todd, D.A. Freer, R.M. Waldren, International Journal of Mass Spectrometry and Ion Processes, Vol. 36, 185.

(TO80) J.F.J. Todd, D.A. Freer, R.M. Waldren, International Journal of Mass Spectrometry and Ion Processes, Vol. 36, 371.

(TO91) J.F.S. Todd, A.D. Penman, International Journal of Mass Spectrometry and Ion Processes, Vol. 106, 1.

REFERENCES

(BR86) J.L. Brand and S.M. George, Surface Science, Vol. 167, p.341 (1986).

(BE91) S.C. Beu, D.A. Laude, International Journal of Mass Spectrometry and Ion Processes, Vol. 104, 109.

(BO90) G. Bollen, R.B. Moore, G. Savard, H. Stolzenberg, Journal of Applied Physics, Vol. 68, 9, 435S.

(BR90) G. Brincourt, R. Catella, Y. Zerega, J. André, Chemistry and Physics Letters, Vol. 174, 6, 626.

(CH80) R. Chattopadhyaya, P K. Ghosh, International Journal of Mass Spectrometry and Ion Processes, Vol. 36, 365.

(CH83) A.D. Chattopadhyay, P.K. Ghosh, International Journal of Mass Spectrometry and Ion Processes, Vol. 49, 253.

(CO87) J.N. Couris, S.S. Brodlet, R.G. Cooks, International Journal of Mass Spectrometry and Ion Processes, Vol. 75, 345.

(CO89) J.N. Couris, J.W. Amy, T.Y. Ridley, R.G. Cooks, International Journal of Mass Spectrometry and Ion Processes, Vol. 88, 97.

(CO90) J.N. Couris, J.S. Brodbelt-Lustig, R.G. Cooks, International Journal of Mass Spectrometry and Ion Processes, Vol. 96, 117.

(CS81) O. Chun-Sing, H.A. Schuessler, Journal of Applied Physics, Vol. 52, 3, 1157.

(DA76) P. Dawson, "Quadrupole Mass Spectrometry and Its Applications", Elsevier Scientific, N.Y., 1976.

(DA88) D.A. Dahl, J.E. Delmore, Simion User's Manual, (1988).

(DE67) H.G. Dehmelt, Advances in Atomic and Molecular Physics,5, 109

(DE87) W.N. Delgass, R.G. Cooks, Science, Vol. 235, 4788, 545.

(DE90) A.M.G. Dezfuli, M.Sc. Thesis, McGill University, unpublished, 1990.

(FR91) I. Franzen, International Journal of Mass Spectrometry and Ion Processes, Vol. 106, 63.

(GA86) R.H. Gabung, G. Romanowski, K.P. Wanczek, International Journal of Mass Spectrometry and Ion Processes, Vol. 69, 153.

(GI91) C.G. Gill, B. Daigle, M.W. Blades, Spectrochimica Acta, Vol. 463, 8, 1227.

(GL89) G.C. Glish, D.E. Goeringer, K.G. Asano S.A. McLuckey, International Journal of Mass Spectrometry and Ion Processes, Vol. 94, 15.

(YO89) J. Yoda, K. Sugiuama, IEEE Transactions on Instruments and Measurements, Vol. 38, 2, 521.